NASA TECHNICAL NOTE

NASA TN D-2558

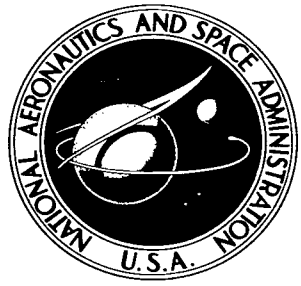

NASA TN D-2558

ANALYSIS OF A DOUBLE FIN-TUBE FLAT CONDENSER-RADIATOR AND COMPARISON WITH A CENTRAL FIN-TUBE RADIATOR

by Henry C. Haller

Lewis Research Center

Cleveland, Ohio

NATIONAL AERONAUTICS AND SPACE ADMINISTRATION • WASHINGTON, D. C. • DECEMBER 1964

ANALYSIS OF A DOUBLE FIN-TUBE FLAT CONDENSER-RADIATOR AND COMPARISON WITH A CENTRAL FIN-TUBE RADIATOR

By Henry C. Haller

Lewis Research Center
Cleveland, Ohio

NATIONAL AERONAUTICS AND SPACE ADMINISTRATION

For sale by the Office of Technical Services, Department of Commerce,
Washington, D.C. 20230 -- Price $2.00

ANALYSIS OF A DOUBLE FIN-TUBE FLAT CONDENSER-RADIATOR AND COMPARISON WITH A CENTRAL FIN-TUBE RADIATOR

by Henry C. Haller

Lewis Research Center

SUMMARY

An analytical study of a flat condenser-radiator with a double fin-tube geometry (closed sandwich) with variable tube side-wall thickness was performed for a Rankine space-power electric-generating system. The analysis of the double fin radiator included consideration of tube and header pressure drops, meteoroid protection for the tubes and headers, along with a detailed presentation of the heat rejection analysis and total weight characteristics. The double fin-tube radiator is compared to a conventional central fin-tube configuration on a heat rejection to weight basis for a four-panel radiator configuration.

Both fin and tube geometries are compared on the basis of the same power level, working fluid temperature, tube and header pressure drop, radiator material, and meteoroid protection criteria. A beryllium radiator for a 1-megawatt system and a columbium alloy radiator for a 500-kilowatt system, both at a radiating temperature of 1700° R, were chosen for the weight and geometry comparisons.

The conclusion reached indicates a substantial weight savings can be realized with the double fin-tube arrangement if the tube side-wall thickness can be reduced as a result of a possible meteoroid bumper effect of the enclosing fins. Weight reductions compared to the central fin-tube geometry of up to 32 to 39 percent were shown to be possible for the maximum reduction in side-wall thickness in the two examples considered. This result further substantiated the preliminary conclusions given in an earlier reference that compared the double and central fin-tube configurations neglecting the effects of headers, pressure drops, tube wall temperature drop, and powerplant thermodynamic cycle considerations. Thus an incentive is offered to further investigate the meteoroid bumper screen concept and its application in the double fin-tube geometry radiator.

INTRODUCTION

The generation of large amounts of electric power in space using the Rankine cycle concept requires that a large amount of waste heat be rejected

from the working fluid. This waste heat is the amount of energy that must be rejected from the working fluid vapor leaving the turbine in order to completely condense it. Since radiation is the only mode of heat transfer for rejecting this energy and since maximum temperatures are limited, the resulting radiator surface areas and weights are generally large. Previous studies on space radiators (refs. 1 to 5) have indicated that a central fin-tube arrangement is feasible since it reduces radiator weight by reducing the prime surface area vulnerable to critical damage by impacting meteoroids. Reference 6 presents the analysis and results of a central fin-tube radiator using flat plate fins of constant cross section.

A preliminary comparison of several fin-tube configurations was carried out in reference 7 that did not include cycle considerations, vapor and liquid headers, and tube and header pressure drops. The results of reference 7 indicated that a substantial weight savings could be obtained by using a double fin tube with reduced rectangular tube side-wall thickness instead of the central or open sandwich fin-tube arrangements. A reduced tube side-wall thickness can result from the assumption that the two fins of the double fin-tube configuration will act as a bumper screen to incident meteoroids, thus allowing some reduction in the thickness of the tube side wall. The double fin-tube configuration is attractive from a structural viewpoint since it provides a rigid structure that has a continuous smooth surface that could be the vehicle skin. These attractive features motivated the need for a more sophisticated analysis.

The purpose of this study is to analyze in a more comprehensive manner the heat rejection and weight characteristics of a double fin-tube configuration with variable rectangular tube side-wall thickness, and to more accurately identify the potential weight savings over radiators with a central fin-tube geometry. The vapor and liquid headers are also included in the geometry analyzed since they directly affect the meteoroid protection requirements of the radiator tubes and can be a significant portion of the total radiator weight. There is also a sizable amount of heat that can be rejected from the vapor header for large power systems (ref. 1). Working fluid pressure drops were also considered for the tubes and headers.

A rectangular cross-section fin was chosen for the analysis and comparison. A one-dimensional approach was taken in the development of the fin energy balance equation with the assumption that the base temperature of the fin is equal to the outer surface temperature of the tube armor. The radiator heat rejection and weight analysis was carried out for two typical Rankine power-planets: a 1-megawatt potassium cycle with a 1700° R beryllium armor and fin radiator, and a 500-kilowatt potassium cycle with a 1700° R columbium alloy radiator. This report presents the results of the heat rejection and weight analysis for the double fin-tube radiator along with a comparison of these results with those given in reference 6 for the central fin-tube configuration.

SYMBOLS

A surface area, sq ft

A_p radiator planform area, sq ft

A_v vulnerable area, sq ft

a penetration correction factor

B constant

C_p specific heat, Btu/(lb)(^oF)

c_a sonic velocity in armor material, $\sqrt{E_a g/\rho_a}$, ft/sec

D tube diameter, ft

E_a Young's modulus of armor material, lb/sq ft

F angle factor, fraction of the energy leaving a surface that is incident upon another surface

F_{VH} vapor header occlusion factor

g units conversion factor, 32.17 ft/sec^2

H incident energy, Btu/(hr)(sq ft)

h heat of condensation, Btu/lb

J mechanical equivalent of heat, 778 (ft)(lb)/Btu

K factor, $(q_b + q_f)/\epsilon\sigma\pi D_i T_b^4$

K_H fluid turning loss factor from header to tubes

k thermal conductivity, Btu/(hr)(ft)(^oR)

L minimum half length of fin, equal to $L^* - R_o$, ft

L^* one-half the tube center to center distance, ft

l actual half length of fin, ft

N number of radiator tubes

N_c conductance parameter, $\sigma l^2 T_b^3/kt$

P cycle fluid pressure, lb/sq ft

P_e powerplant output, kw

P(0) probability of zero punctures

Q heat rejection rate, Btu/hr

Q_b tube radiant heat rejection rate, Btu/hr

Q_f fin radiant heat rejection rate for a fin length $2l$ radiating from both sides, Btu/hr

Q_{rej} total radiator heat rejection rate, Btu/hr

$Qual_3$ vapor header entrance quality

Q_{VH} vapor header heat rejection rate, Btu/hr

q heat rejection per unit length of tube, Btu/hr ft

R radius, ft

R_b tube side wall to tube centerline dimension, $R_b = R_o - \left(1 - \frac{\delta_s}{\delta_a}\right)\delta_a$, ft

$\mathcal{R}$ fraction of flow area occupied by one phase

Re Reynolds number

T temperature, ^oR

T^* vapor saturation temperature at tube inlet, ^oR

t thickness of fin, ft

u velocity of vapor, ft/sec

V velocity of liquid, ft/sec

$\bar{v}$ average meteoroid velocity, ft/sec

W weight, lb

$\dot{W}$ weight flow per tube, lb/sec

$\bar{W}$ panel width, ft

X normalized distance coordinate, x/l

X_{VH} fraction of total heat rejected by the vapor header

X_{tf} fraction of total heat rejected by the tubes and fins

x coordinate measuring distance along lower fin, ft

Y normalized distance coordinate, y/l

y coordinate measuring distance along upper fin, ft

Z	radiator tube length, ft
α,β	constants in penetration formula
δ	tube wall thickness, ft
ϵ	surface hemispherical emissivity
η^*	thermal effectiveness
θ	normalized temperature, T/T_b
μ	viscosity, lb/ft-sec
ρ	density, lb/cu ft (unless otherwise specified)
σ	Stefan-Boltzmann constant, 0.173×10^{-8} Btu/(hr)(sq ft)($^oR^4$)
τ	mission exposure time, days
Φ,χ	two-phase-flow parameters

Subscripts:

a	armor
b	tube base surface
c	tube liner
cond	conduction
F	friction
f	fin
g	vapor phase
i	inside
LH	liquid header
ℓ	liquid
m	momentum
o	outside
P	particle
R	total

rad	radiation
s	side wall
t	tube
tot	total flow, liquid and vapor
VH	vapor header
X	normalized distance coordinate, x/l
x	coordinate measuring distance along lower fin, ft
Y	normalized distance coordinate, y/l
y	coordinate measuring distance along upper fin, ft
0	conditions at tube inlet
1	base surface 1
2	base surface 2
3	radiator inlet conditions

RADIATOR CONFIGURATION AND THERMODYNAMIC CYCLE

The general radiator panel configuration considered for the analysis is shown in figure 1 where the vapor from the turbine exhaust is distributed to the finned tubes by a vapor header. The heat radiated from the vapor header and finned tubes causes the vapor to condense. The condensate is then subcooled and collected in the liquid header before being sent to the condensate pump. This scheme can be modified by dividing the radiator into a number of nonredundant segments, each of which could be treated as a separate entity.

The detailed cross-section drawing of the double fin-tube with variable tube side wall composed of tube liner inserted in an armor block, which provides meteoroid protection, and two rectangular fins is shown in figure 2. The tube liner, which is exposed to the working fluid, must be capable of withstanding possible corrosion. The liner thickness must also be compatible with current fabrication capabilities and structural requirements, and the presence of the liner may also substantially reduce the required armor thickness (ref. 8). The liner thickness is arbitrarily taken as $\delta_c = 0.040\ D_i$ with a minimum wall thickness set at 0.020 inch. The liner thickness was increased as the inside diameter was increased, so as to provide necessary stiffening and strengthening of the radiator tubes.

For the double fin geometry of figure 2, the liner can be damaged by im-

pacting meteoroids in two general ways. The first is by any primary impacts occurring on the outer exposed surfaces of the tube block. These impacts are assumed to obey the conventional armor penetration and damage relations developed for tubes (refs. 8 to 10), with vulnerable area given by $4R_bZN$. Accordingly, the armor thickness δ_a was determined using the criterion of reference 9. The armor thickness, which is a result of the optimization program (ref. 6), is applied in full on the upper and lower surface of the tube. A second damage source can arise from a spray of particles on the armor block side surface $((D_o - 2t)ZN)$ resulting from impacts on the fin surfaces. In view of the bumper action involved and the obliquity of the secondary impacts, however, a reduction will undoubtedly be allowed in the armor thickness required by the tube block side wall to resist the effects of these secondary impacts. Since no specific relations are at present available for the determination of this side-wall thickness, a parametric variation of the δ_s/δ_a is used to examine the effects of reduced side-wall thickness on radiator weight and geometry. The parameter δ_s/δ_a is defined as the fraction of the armor thickness retained on the enclosed side of the tube block.

The vapor header takes the form of a hollow paraboloid whose wall consists of 0.12-inch-thick liner, which was arbitrarily chosen, and whose meteoroid armor protection thickness is the same as that required by the tubes. The parabolic shape insures constant velocity in the header. For simplicity, the liquid header was designed with a constant diameter and a fluid velocity of 4 feet per second, so that a very low pressure drop would result. The liner for the liquid header follows the same schedule with the inside diameter as do the tube liners. However, a maximum liner thickness is set at 0.12 inch. The liquid header also has meteoroid armor.

The assumptions given herein for the double fin-tube radiator geometry, with the exception of the fin-tube configuration, also hold for the central fin tube that was analyzed in reference 7 and shown in figure 3.

The thermodynamic cycle used in this analysis is the Rankine cycle, which uses a working fluid that undergoes a change of phase. The working fluid is condensed in the radiator, which results in a near isothermal condition prevailing in the tubes and vapor header. In order to show sample results and compare the two fin-tube geometries on a heat rejection per unit weight and on a radiator geometry basis, two power levels were chosen. Potassium was chosen as the working fluid in the cycle for both power levels with a peak turbine inlet temperature of 2460° R and a radiator temperature of 1700° R. It was also specified that the radiator tubes would subcool the working fluid 100° R. Additional cycle requirements such as turbine and generator efficiencies were set at 0.75 and 0.90, respectively, with 10 percent of the generator output required for accessories and controls. The emittance of the radiator was taken to be 0.90, and the effective sink temperature for the radiator was assumed to be 0° R. The foregoing values plus the cycle temperatures, working fluid, and the power level chosen for the analysis and comparison enabled the determination of the total heat rejection rate and the mass flow rate of the working fluid for the radiator design inputs. Additional information required from the cycle analysis is the quality of the working fluid entering the vapor header. The analysis of the thermodynamic cycle used is given in detail in reference 6.

HEAT-TRANSFER ANALYSIS

Approach and Assumptions

The analysis considers the general case of two rectangular profile fins of length l attached to a tube enclosed in an armor block forming a double fin configuration as shown in figure 2. Energy input to the fin is comprised of heat conduction along the fin from the two tube side-wall surfaces. For any specific choice of L/R_o the fin length l as shown in figure 2 will depend on the value of tube side-wall thickness.

The specific assumptions used in the development of the heat-transfer relations for the double fin-tube geometry as well as the central fin-tube geometry are

(1) Radiator emittance is constant with temperature.

(2) For the determination of radiator temperature variation the radiator surfaces act as blackbodies with incident and emitted radiation governed by Lambert's cosine law.

(3) Hemispherical radiation to space from both outer surfaces of the radiator to a 0° R space sink temperature.

(4) The base surface temperature of the fin is assumed constant along the length of the tube and equal to the tube block outer surface temperature.

(5) Steady-state one-dimensional heat flow exists in the fins and tube block.

(6) Material properties are constant along the length of fin and tube block and are evaluated at the fin base temperature.

(7) The development of the fin and tube angle factors for the radiant interchange between fin and tube side walls is based on an infinite length of tube and fin, with fin thickness assumed negligible in the development.

(8) The inside tube wall temperature is circumferentially uniform and equal to the stagnation temperature of the fluid at the inlet of the header.

Tube Wall Temperature Drop

Since the tube block will have thick walls due to the armor required for meteoroid protection, a significant temperature drop will occur across the block. The assumed heat-transfer paths and the various fin and tube block temperatures are shown in figure 4. The inside tube wall temperature T^* is determined from reference 6 as

$$T^* = T_3\left(1 - \frac{1}{2}\frac{K_H u_o^2}{Jgh}\right) \tag{1}$$

where T_3 is the radiator fluid stagnation temperature at the header inlet in degrees Rankine and u_0 is the tube inlet vapor velocity. The turning loss factor K_H in equation (1) was set at 1.15 (ref. 6).

The relation between the tube inside surface temperature and the tube block outer surface temperature is based on a simplified approach that assumed heat is transferred from the tube inner surface to the exposed surface of the tube block by one-dimensional conduction. This heat path was chosen since it represents the greatest flow of energy. The heat transmission by conduction is assumed to travel a distance δ_a through a cross-sectional area $2R_b\,dZ$. The expression for the heat conduction is

$$dq_{cond} = \frac{2kR_b}{\delta_a}(T^* - T_b)dZ \tag{2}$$

For simplicity it is assumed that the temperature drop $T^* - T_b$ is governed primarily by the radiant heat transfer from the exposed surface of the block (neglecting the conduction to the fins). The expression for radiation from one surface element may be written as

$$dq_{rad} = 2\sigma\epsilon R_b T_b^4\,dZ \tag{3}$$

When equations (2) and (3) are combined for $dq_{cond} = dq_{rad}$, the resultant equation for the approximate temperature drop through the tube block wall is given as

$$\sigma\epsilon\delta_a T_b^4 + k(T_b - T^*) = 0 \tag{4}$$

The temperature T_b obtained from equation (4) is then used in the development of the fin heat-transfer relations. The temperature of the tube side wall is also assumed to be equal to the temperature of the tube block exposed surface T_b regardless of the thickness of the tube side wall (all values of δ_s/δ_a).

Fin Temperature Profile

Formulation of equations. - Considering an element of the fin surface in figure 2 and employing the previous assumptions, the law of energy conservation for an element can be expressed as the energy balance between the net heat transfer due to conduction and radiation (ref. 11):

$$dQ_{cond} + dQ_{rad} = 0 \tag{5}$$

The net internal heat conduction through the element of thickness t and length Z is expressed as

$$dQ_{cond} = \frac{d}{dx}\left(-ktZ\,\frac{dT}{dx}\right)dx \tag{6}$$

The net radiant heat rejection from both sides of the element of the fin is composed of its emission minus the incident energy. This expression is given as

$$dQ_{rad} = \left(2\sigma T_x^4 - H_x\right)dA_x \tag{7}$$

The incident energy term H_x in equation (7) is composed of the incident energy from the two side walls to an element of area on the fin

$$\sigma T_b^4\left(F_{dA_x\text{-}1} + F_{dA_x\text{-}2}\right) \tag{8a}$$

and the energy leaving an opposing fin surface incident upon the other

$$\int_{y=0}^{2l} \sigma T_y^4 \, dF_{dA_x\text{-}dA_y} \tag{8b}$$

Substitution of expressions (8a) and (8b) into equation (7) yields

$$dQ_{rad} = \left[2\sigma T_x^4 - \sigma T_b^4\left(F_{dA_x\text{-}1} + F_{dA_x\text{-}2}\right) + \int_{y=0}^{2l} \sigma T_y \, dF_{dA_y\text{-}dA_y}\right]dA_x \tag{9}$$

Introducing equations (6) and (9) into equation (5) and the dimensionless variables

$$X = \frac{x}{l}$$

$$Y = \frac{y}{l}$$

$$\theta = \frac{T}{T_b}$$

$$N_c := \frac{\sigma T_b^3 l^2}{kt}$$

yield the expression

$$\frac{1}{N_c}\frac{d^2\theta}{dX^2} = 2\theta^4(X) - \left(F_{dA_X\text{-}1} + F_{dA_X\text{-}2}\right) - \int_0^2 \theta^4(Y) dF_{dA_X\text{-}dA_Y} \tag{10}$$

The angle factors in equation (10) are evaluated using a relation (ref. 12, eq. (31-58)) that applies to parallel surfaces of infinite length. For the configuration of figure 2 the angle factors in question are given as

$$dF_{dA_X-dA_Y} = \frac{2\left(\frac{R_o}{l}\right)^2}{\left[(Y - X)^2 + 4\left(\frac{R_o}{l}\right)^2\right]^{3/2}} dY \tag{11}$$

$$F_{dA_X-1} = \frac{1}{2}\left\{1 - \frac{X}{\left[X^2 + 4\left(\frac{R_o}{l}\right)^2\right]^{1/2}}\right\} \tag{12}$$

$$F_{dA_X-2} = \frac{1}{2}\left\{1 - \frac{2 - X}{\left[(2 - X)^2 + 4\left(\frac{R_o}{l}\right)^2\right]^{1/2}}\right\} \tag{13}$$

Introduction of equations (11), (12), and (13) and the symmetry of the temperature distribution about $x = l$, that is, $T(x) = T(2l - x)$, into equation (10) yield the expression

$$\frac{1}{N_c}\frac{d^2\theta}{dX^2} = 2\theta^4(X) - 1 + \frac{1}{2}\left\{\frac{X}{\left[X^2 + 4\left(\frac{R_o}{l}\right)^2\right]^{1/2}} + \frac{2 - X}{\left[(2 - X)^2 + 4\left(\frac{R_o}{l}\right)^2\right]^{1/2}}\right\}$$

$$- 2\left(\frac{R_o}{l}\right)^2 \int_0^1 \theta^4(Y)dY\left\{\frac{1}{\left[(Y - X)^2 + 4\left(\frac{R_o}{l}\right)^2\right]^{3/2}} + \frac{1}{\left[(2 - Y - X)^2 + 4\left(\frac{R_o}{l}\right)^2\right]^{3/2}}\right\} \tag{14}$$

where the actual fin length l is given by the expression (fig. 2)

$$l = L + \left(1 - \frac{\delta_s}{\delta_a}\right)\delta_a \tag{15}$$

Computational procedure. - It was necessary to use numerical techniques to solve equation (14) for the temperature profile of the fin of length l. The numerical solutions were carried out on an IBM 7094 electronic digital computer.

The second order differential equation $d^2\theta/dX^2 = B\theta^4 + f(X)$ was solved for the θ profile in the interval $X = 0$ to $X = 1$. The boundary conditions are $\theta = 1$ at $X = 0$ and $d\theta/dX = 0$ at $X = 1$, where B is a constant and $f(X)$ is a function of X. Kalaba's method was used and is now described.

The term θ^4 was approximated by a linear function of θ, namely by the first two terms of its Taylor series expansion. Central differences were used to obtain an expression for $d^2\theta/dX^2$. At each point of a mesh on the interval $X = 0$ to $X = 1$, the equation $d^2\theta/dX^2 = B\theta^4 + f(X)$ was thus approximated as a linear function of θ. The set of resulting tridiagonal linear equations was reduced to two-diagonal form, and these were then solved for the θ profile by backward substitution. An initial θ profile guess was used, and each successive iteration yielded approximately one decimal place of accuracy. Solutions were obtained as a function of the input parameters N_c and l/R_o.

Temperature profile results. - Each solution of the fin energy equation, which is independent of power and temperature level or tube inside diameter, provided a temperature distribution along the fin. Results are plotted in figure 5 as a function of position X on the fin for several parametric values of N_c and l/R_o. It is seen that the temperature drop along the fin is very small when the conductance parameter N_c is small, which indicates a low thermal resistance of the fin. Additionally, there is little effect of l/R_o when N_c is small, although a greater temperature drop occurs with increasing l/R_o ratio. This holds regardless of the choice of the tube wall thickness ratio δ_s/δ_a, since only the l/R_o ratio is considered in the development of equation (14).

Radiator Effectiveness

Fin heat rejection. - After the temperature distribution and the slope of the temperature distribution curve at $X = 0$ have been determined, the net heat transferred by the fin can be calculated. The rate of heat loss from the fin outer surface at any point x on the fin from a differential area $NZ\,dx$ is $\sigma\epsilon ZNT_x^4\,dx$. The overall rate of heat loss Q_f from the pair of fins that forms the double fin tube is

$$Q_f = 2\int_0^{2l} \epsilon\sigma ZNT_x^4\,dx = 4\sigma ZNlT_b^4\epsilon\int_0^1 \theta^4(X)dX \qquad (16)$$

This equation is evaluated using the solutions of the fin energy equation (14). Comparison of this fin energy rejection to the total heat loss from both sides of an isothermal fin-tube section of length $2(l + R_b)$ can be expressed in dimensionless terms as

$$\eta_f^* = \frac{Q_f}{4\epsilon\sigma Z N l\left(1 + \frac{R_b}{l}\right)T_b^4} = \frac{\int_0^1 \theta^4(X)dX}{1 + \frac{R_b}{l}} \tag{17}$$

where

$$\frac{R_b}{l} = \frac{R_o - \left(1 - \frac{\delta_s}{\delta_a}\right)\delta_a}{L + \left(1 - \frac{\delta_s}{\delta_a}\right)\delta_a} \tag{18}$$

and $\theta(X)$ is a function of X for specific values of δ_s/δ_a, L/R_o, and N_c. Equation (17) can be defined as the thermal effectiveness of the double fin.

The results obtained from the solutions of equation (17) for fin effectiveness are presented for an example case in figure 6 as a function of L/R_o for parametric values of N_c and δ_s/δ_a. In the aforementioned equations describing fin effectiveness (eqs. (17) and (18)), the tube wall thickness δ_a must be known in order to obtain solutions. In order to obtain the actual value of δ_a, the tube inside diameter D_i, tube liner thickness δ_c, power and temperature level, materials, meteoroid protection criteria, tube and header pressure drop, and definition of radiator tube vulnerable area must be specified. Thus, solutions for equation (17) require complete solutions for the entire radiator. Such radiator solutions will be described in detail in the section RADIATOR WEIGHT AND GEOMETRY.

Inspection of the curves in figure 6 reveals that for any fixed value of L/R_o and δ_s/δ_a the fin effectivenss decreases with increasing values of N_c. The fin effectiveness is also seen to decrease with increasing δ_s/δ_a at constant N_c. When L/R_o equals zero the value of fin effectiveness does not equal zero when the value of δ_s/δ_a is other than 1. This is due to an increase in the fin length caused by the reduction of tube side-wall thickness for any choice of L/R_o ratio. Thus, at L/R_o equal to zero, a fin remains of length $l = \delta_a - \delta_s$.

Tube heat rejection. - The net heat loss from the external surface of the tube block is just its radiant emission since there is no incident energy from other parts of the system. This energy rejection when compared to the total heat loss from both surfaces of an isothermal fin-tube section of length $2(l + R_b)$ can be defined as the thermal effectiveness of the exposed surface of the tube. This expression is

$$\eta_b^* = \frac{Q_b}{4\sigma\epsilon N Z l\left(1 + \frac{R_b}{l}\right)T_b^4} = \frac{1}{1 + \frac{l}{R_b}} \tag{19}$$

where l/R_b is defined in terms of R_o, L, δ_a, and δ_s/δ_a in equation (18). The heat radiation from the tube side-wall surfaces is already included as a contribution to the heat radiated from the fin, since in effect the radiant interchange acts in a manner similar to the heat conduction down the fin. This aspect is fully explained in reference 11. Solutions for equation (19) also require values of armor thickness δ_a and thus are a result of the radiator calculation procedure for the double fin-tube block configuration.

Results of equation (19) for tube effectiveness are shown plotted for an example case in figure 7. Tube thermal effectiveness is seen to decrease as L/R_o is increased, which indicates a decrease in the relative importance of the tube portion as the fin length increases. Decreasing the tube wall ratio δ_s/δ_a also results in a reduced tube effectiveness, which is caused by a reduction in the tube block outer surface area and thus the energy it can reject to space. It is also seen from the figure that for an L/R_o ratio equal to zero the tube effectiveness does not equal 1 if the ratio δ_s/δ_a is less than 1. This is brought about because a fin of length $\delta_a - \delta_s$ remains (see eq. (15)).

Total fin-tube heat rejection. - For calculation purposes, it is desirable to formulate the total fin-tube thermal effectiveness that can be determined by summing the results of equations (17) and (19) for fin effectiveness and tube effectiveness, respectively. This expression is

$$\eta_R^* = \frac{Q_f + Q_b}{4\sigma\epsilon NZl\left(1 + \frac{R_b}{l}\right)T_b^4} = \frac{1}{1 + \frac{l}{R_b}}\left[1 + \frac{l}{R_b}\int_0^1 \theta^4(X)dX\right] \qquad (20)$$

Figure 8 shows a plot of total fin-tube effectiveness η_R^* against L/R_o ratio for several choices of conductance parameter N_c and tube block side-wall ratio δ_s/δ_a for an example case. Inspection of the curves shown in figure 8 reveals that for any fixed value of L/R_o and N_c the total fin-tube thermal effectiveness decreases as the δ_s/δ_a ratio decreases. This is reasonable since as the δ_s/δ_a ratio decreases the amount of isothermal base surface decreases. The fin-tube effectiveness is also reduced by increasing the conductance parameter or by increasing the L/R_o ratio.

Negligible variation in the magnitude of η_R^* was observed for the two power levels chosen for the comparison. Thus the curves given in figure 8 for the 500-kilowatt case also apply for the 1-megawatt power level case. It was also noticed that variations of the tube inside diameter had no appreciable effect on the value of η_R^* at a specific value of the L/R_o ratio, the δ_s/δ_a ratio, and the conductance parameter N_c.

PRESSURE DROP CONSIDERATIONS

Another factor that is required to determine the geometry and weight of a radiator is the pressure drop determination in the radiator tubes and headers. This aspect of radiator design helps to determine the vapor header geometry and

the required tube diameter, the tube length, and the number of tubes. The equations presented are for a Rankine cycle condenser-radiator which assumed that vapor flow in the vapor header to be of the same quality as the turbine exhaust, two-phase flow in the radiator tubes and all-liquid flow in the liquid header. The development of the equations given in this section are given in reference 6.

Vapor header. - The determination of the pressure drop in the vapor header is simplified by assuming that only the gas phase affects the pressure drop. This pressure drop is expressed as a ratio of ΔP to the header inlet pressure P_3 with the resulting ratio kept constant for comparative purposes. This equation, which is for turbulent flow, is

$$\left(\frac{\Delta P}{P_3}\right)_{VH} = \frac{0.00357\ \rho_g u_{VH}^2 \overline{W}}{2P_3 Re^{0.2} D_{VH}} \tag{21}$$

where u_{VH} is the uniform vapor velocity in the parabolic header (based on the turbine exhaust quality and neglecting the flow area occupied by the liquid) and Re is the vapor Reynolds number based on the vapor header maximum diameter D_{VH}. The value of D_{VH} is obtained from the expression

$$D_{VH} = \left(\frac{2\dot{W}\ Qual_3}{\rho_g \pi u_{VH}}\right)^{1/2} \tag{22}$$

and the total panel width $\overline{W}$ in equation (21) is

$$\overline{W} = \frac{NR_o}{2}\left(1 + \frac{L}{R_o}\right) \tag{23}$$

The term $Qual_3$ in equation (22) is the vapor quality at the entrance to the vapor header. The number of condensing tubes N in the previous equation is determined from the tube pressure drop analysis in conjunction with the optimization procedure used for this fin-tube geometry.

The amount of heat rejected to space from the parabolic vapor header is determined from the following expression:

$$Q_{VH} = Q_{rej} X_{VH} = 2.09\ \epsilon\sigma D_{VH} F_{VH} \overline{W} T_3^4 \tag{24}$$

where the factor F_{VH} is defined as the vapor header occlusion factor for radiant emission to space and given a value of 0.85 for this analysis (ref. 13). The analysis and results of reference 13 (fig. 4) although primarily for tubes and fins are assumed valid for the occlusion of the header-panel arrangement shown in figure 1.

Radiator Tubes

The pressure drop in the radiator tubes where flowing vapor is condensing

was computed from a combination of several basic flow and energy equations that are given in detail in reference 6. The flow model (ref. 14) used assumed that at any given section perpendicular to the flow direction, the temperature and pressure in both the liquid and vapor are uniform and the same for both phases. This flow model also assumed turbulent flow with liquid and vapor velocities uniform in each phase at a given cross section, but that the two velocities were not necessarily equal. Pressure drops were computed for a series of incremental tube lengths, and the pressure drop for the whole tube was obtained by summing the incremental drops.

The total change in pressure for an entire radiator tube is comprised of a frictional and a momentum component. The friction pressure drop is described by the expression

$$dP_F = -\Phi_g^2 Re_g^{1.8}\left(\frac{0.092\ \mu_g^2\ dx}{gD_i^3\rho_g}\right) \tag{25}$$

where $Re = 4\dot{W}_g/\pi D_i \mu_g$ and Φ_g is a function of X. The differential form of the change in pressure due to a change in momentum is

$$-dP_m = \frac{1}{gA}\left[d\left(\rho_\ell A_\ell V^2\right) + d\left(\rho_g A_g u^2\right)\right] \tag{26}$$

A third relation is required that relates the increment of tube length and the increment of condensate formed:

$$d\dot{W}_\ell = \frac{\dfrac{K\epsilon\sigma\pi D_i T_b^4}{3600}\,dx + \dfrac{C_{p\ell}\dot{W}_\ell + C_{pg}\dot{W}_g}{Jh\rho_g}\,T\,dP_F}{h - \dfrac{V^2}{Jg}\left(1.5 - \dfrac{0.9\ d\mathcal{R}_\ell}{dX}\dfrac{X\dot{W}_{tot}}{\mathcal{R}_\ell\dot{W}_g}\right) + \dfrac{u^2}{gJ}\left(1.5 - \dfrac{0.9\ d\mathcal{R}_\ell}{dX}\dfrac{X\dot{W}_{tot}}{\mathcal{R}_g\dot{W}_\ell}\right) - \dfrac{C_{p\ell}\dot{W}_\ell + C_{pg}\dot{W}_g}{Jh\rho_g}\,T\,\dfrac{dP_m}{d\dot{W}_\ell}} \tag{27}$$

where for the double fin-tube radiator the definition of K is

$$K = 4\,\frac{R_b\eta_R^*}{\pi D_i}\left(1 + \frac{l}{R_b}\right) \tag{28}$$

Equations (25), (26), and (27) along with equation (1) are solved simultaneously for dW, dP_m, and dP_F. The total change in pressure for each increment can then be found from the relation

$$dP = dP_m + dP_F \tag{29}$$

and the total pressure change for the entire radiator tube can be found by

summing the incremental changes. For comparative purposes, the total tube pressure drop is expressed as the ratio of pressure drop to the tube inlet pressure.

The pressure drop associated with turning the vapor from the vapor header into the radiator tubes and accelerating the flow can be calculated from the expression

$$\Delta P_{entrance} = K_H \frac{1}{2} \rho_g \frac{u_o^2}{g} \tag{30}$$

where the tube entrance loss factor K_H is given the same value used in equation (1).

Liquid Header

The pressure drop in the liquid header is obtained by applying Fanning's equation with a friction factor for turbulent flow. This expression is

$$\Delta P_{LH} = \frac{0.00102\ \rho_{\ell} V_{VH}^2 \overline{W}}{D_{LH}(Re_{\ell})^{0.2}} \tag{31}$$

where Re is the Reynolds number corresponding to the maximum liquid velocity V_{LH} that, in these calculations, was taken as 4 feet per second. The liquid header diameter D_{LH}, which is assumed constant, is determined by applying the continuity equation at the header exit to give the expression

$$D_{LH} = \left(\frac{\dot{W}}{\pi \rho_{\ell} V_{LH}} \right)^{1/2} \tag{32}$$

RADIATOR WEIGHT AND GEOMETRY

The heat-rejection analysis of the fin and the tube was nondimensionalized so that the results could be used for general design purposes. Using the previous results for analyzing the merits of the variable tube wall double fin-tube configuration in radiator designs is impractical without consideration of the total weight of the vapor and liquid headers as well as the tubes and fins. It is necessary, therefore, to consider the ratio of heat rejection per unit weight Q_{rej}/W and the influencing effects of radiator geometry limitations on the maximum heat rejection per unit weight.

Armor Thickness

In order to determine both radiator weight and geometry, the effects of meteoroid penetration must be considered on both the tubes and headers. This will dictate the required armor protection thickness needed for the radiator.

The tube armor thickness δ_a is determined using the meteoroid protection criteria given in reference 9, which is based on a comprehensive appraisal of the available data and theories concerning the meteoroid penetration phenomenon. According to reference 9, the resultant equation for the armor thickness δ_a is given by the expression

$$\delta_a = 2a\left(\frac{\rho_P\ 62.45}{\rho_a}\right)^{1/2}\left(\frac{\bar{v}_P}{c_a}\right)^{2/3}\left(\frac{6.747\times10^{-5}}{\rho_P}\right)^{1/3}\left[\frac{\alpha A_V \tau}{-\ln P(0)}\right]^{1/3\beta}\left(\frac{1}{\beta + 1}\right)^{1/3\beta} \tag{33}$$

where in the previous equation

$a = 1.75$

$\beta = 1.34$

$\rho_P = 0.44$ g/cu cm

$\bar{v}_P = 98{,}400$ ft/sec

$\alpha = 0.53\times10^{-10}$ $g^{\beta}/(\text{sq ft})(\text{day})$

Insertion of these constants into equation (33) along with utilizing Young's modulus in the definition of sonic velocity of the material yields the more compact form

$$\delta_a = \frac{1.48}{\rho_a^{1/6}E_a^{1/3}}\left[\frac{A_V \tau}{-\ln P(0)}\right]^{0.249} \tag{34}$$

The total exposed area to be protected by direct impacts A_V is assumed to be the outer surface of the vapor header and the projected area of the tube block. The liquid header contribution is assumed to be negligible since its surface area is small compared to that of the vapor header. Thus

$$A_V = A_t + A_{VH} \tag{35}$$

The radiator tube projected area is given by the expression

$$A_t = 4R_b NZ = \frac{Q_{rej} X_{tf}}{\sigma\epsilon T_b^4\left(1 + \frac{l}{R_b}\right)\eta_R^*} \tag{36}$$

where l/R_b is obtained from equation (18) and η_R^* from equation (20). The fraction of the total radiator heat that is rejected by the tubes and fins X_{tf} is defined by the expression

$$X_{tf} = \frac{Q_t + Q_f}{Q_{rej}} = 1 - X_{VH} \tag{37}$$

The vulnerable area of the vapor header is assumed to be its full surface area and is given as

$$A_{VH} = \frac{Q_{rej} X_{VH}}{\sigma \epsilon F_{VH} T_3^4} \tag{38}$$

where F_{VH} is the occlusion factor for the effect of the radiator panel on the heat rejection of the vapor header surface.

Combining equations (35) to (38) yields

$$A_v = \frac{Q_{rej}}{\sigma \epsilon} \left[\frac{1 - X_{VH}}{\left(1 + \frac{l}{R_b}\right) \eta_R^* T_b^4} + \frac{X_{VH}}{F_{VH} T_3^4} \right] \tag{39}$$

Weight Ratio

The total heat rejection per unit weight of a fin-tube radiator can be expressed as

$$\frac{Q_{rej}}{W} = \frac{\frac{Q_{rej}}{NZ}}{\frac{W}{NZ}} \tag{40}$$

where for radiation from both sides of the radiator and from the vapor header

$$\frac{Q_{rej}}{NZ} = \sigma \epsilon \left[4 R_o T_b^4 \eta_R^* \left(1 + \frac{L}{R_o}\right) + \frac{2.09 D_{VH} F_{VH} \bar{W} T_3^4}{NZ} \right] \tag{41}$$

Insertion of equation (23) into equation (41) yields the following form of the total radiator heat rejection per unit length of tube:

$$\frac{Q_{rej}}{NZ} = \sigma \epsilon R_o \left(1 + \frac{L}{R_o}\right) \left(4 \eta_R^* T_b^4 + 1.045 \frac{D_{VH} F_{VH} T_3^4}{Z} \right) \tag{42}$$

where the outside tube diameter (block width) D_o can be expressed in terms of the liner thickness δ_c, the inside tube diameter D_i, and the armor thickness δ_a and can be given as

$$D_o = D_i + 2\delta_c + 2\delta_a \tag{43}$$

The total weight of the radiator is comprised of the individual weights of

the vapor header, the liquid header, and the tube-fin panel. The weight of the liquid inventory in the subcooler portion of the radiator tubes is neglected since the subcooler length is small. The vapor header weight is given by (ref. 6)

$$W_{VH} = \frac{4\overline{W}}{3}\pi\left[\left(D_{VH} + \delta_{VH_c}\right)\delta_{VH_c}\rho_c + \left(D_{VH} + 2\delta_{VH_c} + \delta_a\right)\delta_a\rho_a\right] \tag{44}$$

and that of the liquid header and condensate by

$$W_{LH} = 4\pi\overline{W}\left[\frac{\rho_{\ell}D_{LH}^2}{4} + \rho_c\delta_{LH_c}\left(D_{LH} + \delta_{LH_c}\right) + \rho_a\delta_a\left(D_{LH} + \delta_a + 2\delta_{LH_c}\right)\right] \tag{45}$$

The fin and tube panel weight can be calculated using the expression

$$W_{tf} = 4\ell t\rho_f NZ + \rho_c\frac{\pi}{4}NZ\left[(D_i + 2\delta_c)^2 - D_i^2\right] + NZ\rho_a\left[4R_oR_b - \frac{\pi}{4}(D_i + 2\delta_c)^2\right] \tag{46}$$

When $t = \sigma\ell^2T_b^3/kN_c$, D_o from equation (43), ℓ from equation (15), and $R_b = R_i + \delta_c + (\delta_s/\delta_a)\delta_a$ are introduced into equation (46), the equation for the tube and fin panel weight becomes

$$W_{tf} = \frac{4\rho_f NZ\sigma T_b^3}{kN_c}\left[\frac{L}{R_o} + \left(1 - \frac{\delta_s}{\delta_a}\right)\frac{\delta_a}{R_o}\right]^3(R_i + \delta_c + \delta_a)^3 + \rho_c\pi\delta_c NZ(D_i + \delta_c)$$

$$+ \rho_a NZ\left\{2(D_i + 2\delta_c + 2\delta_a)\left[R_i + \delta_c + \left(\frac{\delta_s}{\delta_a}\right)\delta_a\right] - \pi(R_i + \delta_c)^2\right\} \tag{47}$$

The total radiator weight is then obtained by summing the results of equations (44), (45), and (47). The denominator of equation (40) can be found by dividing the total radiator weight by the total tube length NZ. This result along with the results of equation (42) when inserted into equation (40) yield the radiator heat rejection per unit weight. The peak value of Q_{rej}/W can then be obtained by plotting the results of equation (40) as a function of L/R_o for specific values of conductance parameter N_c and tube side-wall ratio δ_s/δ_a.

Panel Geometry

In addition to the important aspect of minimizing weight for practical radiator designs, it is also of interest in most cases to investigate the geometry of the radiator as it might affect the integrating of the vehicle and radiator. Planform area, aspect ratio, and fin thickness are three facets of the geometry of the radiator panel that must be determined in order to satisfy radiator-space vehicle integration and structural and fabricational require-

ments of the fin-tube configuration.

Radiator planform area A_p is obtained from the equation

$$A_p = 2NZ(L + R_o) = \frac{Q_{rej} X_{tf}}{2\sigma\epsilon T_b^4 \eta_R^*} \tag{48}$$

It is seen from this equation that planform area will vary inversely with overall fin-tube thermal effectiveness η_R^* for a specific choice of power and temperature level. The planform area will generally increase with increasing L/R_o because η_R^* decreases as the L/R_o ratio is increased (fig. 8).

Another interesting factor with respect to the geometry of the radiator is the magnitude of the fin thickness. Radiator applications might require that the fin have structural or fabricational qualities that could result in nonoptimum weights and dimensions. Fin thickness t for the closed sandwich configuration can be calculated from the expression

$$t = \frac{\sigma T_b^3 l^2}{kN_c} \tag{49}$$

The panel aspect ratio, which is defined as the ratio of panel width $\overline{W}$ to tube length Z, is obtained by using equation (23) for $\overline{W}$ and the results of the pressure drop calculations for Z.

Method of Solution

Simultaneous solution of equations (4), (20), (21), (29), (33), and (39) requires inputs of inside tube diameter D_i, tube and vapor header pressure drop ratios, power level, temperature level, and the properties of the materials and cycle fluid. This results in values of the parameters δ_a, T_b, X_{VH}, N, and u_o for a selected variation of L/R_o, conductance parameter N_c, and the tube side-wall ratio δ_s/δ_a.

Important results required for weight and geometry calculations will include the number of tubes N, tube length Z, tube outside radius R_o, panel width $\overline{W}$, and the inside diameter of the vapor header D_{VH}. An electronic digital computer was used to obtain the desired results that required an iterative type solution.

RESULTS AND DISCUSSION

Calculation Inputs

Calculations making use of the resultant equations developed in the analysis for the double fin-tube geometry require inputs such as inside tube diameter, radiator vapor inlet temperature, cycle power level and conditions, mate-

rials of construction, meteoroid protection criteria, tube block side-wall thickness ratio, and pressure drop in the tubes and header in order to completely specify a radiator solution. For this reason two specific cases are used in order to show the effects of some of the previously mentioned variables on heat rejection per unit weight and on radiator geometry.

The first case considered is a 1-megawatt electrical output powerplant with the radiator at 1700° R. The tube armor and the fin were assumed to be made of beryllium, and the tube liner was assumed to be a columbium alloy. The second case is a 500-kilowatt system with the radiator at 1700° R. For this case, the tube armor, tube liner, and the fin were all taken to be columbium - 1-percent zirconium alloy. These two cases both used a peak cycle temperature of 2460° R and potassium as the cycle fluid. Inside tube diameters of 3/8, 1/2, 5/8, 3/4, and 1 inch were chosen with tube lengths increased to allow 100° R of subcooling. A 500-day mission time and a probability of no puncture P(0) of 0.995 were chosen for the calculation of meteoroid protection thickness. Pressure drop ratios for the two cases were set at $\Delta P/P = 0.02$ for the vapor header and $\Delta P/P = 0.05$ for the radiator tubes. The emittance of the surface coating on the fins, tubes, and headers was taken to be 0.90. Radiator material properties were assumed constant with temperature and evaluated at 1700° R. The all columbium alloy radiator had a density of 530 pounds per cubic foot, thermal conductivity of 34 Btu per hour per foot per °F, and a modulus of elasticity of 0.202×10^{10} pounds per square foot. The beryllium radiator used a density of 115 pounds per cubic foot, a thermal conductivity of 51.5 Btu per hour per foot per °F, and a modulus of elasticity of 0.397×10^{10} pounds per square foot. The beryllium radiator used a columbium liner with the material properties previously mentioned.

Calculations using the given inputs and specifications were also made for the central fin-tube geometry that used the method described in reference 6.

Radiator Weight

Radiator heat rejection per unit weight Q_{rej}/W was plotted for each value of inside tube diameter D_i and tube block side-wall ratio δ_s/δ_a chosen for the comparison over a range of the parameters N_c and L/R_o. Results showing the variation in heat rejection rate per unit weight as a function of L/R_o for several values of conductance parameter N_c are shown plotted for two sample cases in figure 9. The figure shows results for the tube block side-wall thickness to tube armor thickness ratio δ_s/δ_a equal to 0.5 with tube inside diameters of 3/8 and 5/8 inch chosen for the 500-kilowatt and 1-megawatt cases, respectively. Each constant N_c curve is seen to peak at a specific value of L/R_o with the value of the L/R_o at peak Q_{rej}/W increasing as N_c is increased.

Plotting the maxima for each N_c curve of figure 9 and the additional results for the $\delta_s/\delta_a = 0$ and 1.0 cases yield a performance map (fig. 10) that plots peak heat rejection per unit weight against L/R_o. It is seen from figure 10 that decreasing the armor block side-wall thickness results in a sub-

stantial increase in the value of Q_{rej}/W. According to figure 10, the maximum Q_{rej}/W occurs at an N_c approximately equal to 0.75 for the 500-kilowatt system at a tube inside diameter of 3/8 inch. The results for the 1-megawatt system indicate this maximum also occurs near an $N_c = 0.75$ for a near optimum tube inside diameter of 5/8 inch.

Plotting the maxima of figures 10(a) and (b) on figures 11(a) and (b), respectively, and the results for additional inside tube diameters yield the maximum value of Q_{rej}/W and its corresponding inside tube diameter for the three values of δ_s/δ_a chosen for the comparison. The curves given in figure 11(a) for the 500-kilowatt case indicate that maximum Q_{rej}/W for any choice of δ_s/δ_a occurs at a tube inside diameter between 3/8 and 1/2 inch with the Q_{rej}/W curve relatively flat in this region. Maximum Q_{rej}/W occurred at a diameter between 1/2 and 5/8 inch for the 1-megawatt system as shown in figure 11(b).

The weight results of the double fin-tube configurations are compared to the central fin-tube results in figures 11(a) and (b) in order to show the desirability of the double fin-tube with reduced tube side-wall thickness. It is observed from figure 11 that the central fin-tube configuration has a larger heat rejection per unit weight than the double fin-tube with $\delta_s/\delta_a = 1.0$. For the 500-kilowatt case, the double fin tube with $\delta_s/\delta_a = 0.5$ affords an 11-percent weight advantage at maximum Q_{rej}/W over the central fin tube, and a maximum upper limit of 39 percent when $\delta_s/\delta_a = 0$. The radiator weight per kilowatt of electrical power for the 500-kilowatt case using a columbium radiator is 10.2, 15.0, and 19.0 pounds per kilowatt for the $\delta_s/\delta_a = 0$, 0.5, and 1.0 cases, respectively.

The percentage weight savings are reduced for the 1-megawatt power level with the beryllium radiator and are 8 percent for the $\delta_s/\delta_a = 0.5$ case and 32 percent for the $\delta_s/\delta_a = 0$ case. For this power level, the specific weight was 3.50, 4.68, and 5.73 pounds per kilowatt for the $\delta_s/\delta_a = 0$, 0.5, and 1.0 cases, respectively. The beryllium radiator has a smaller percent increase in Q_{rej}/W than the columbium radiator because there is less relative weight in the beryllium armor.

The conclusions reached in figure 19 of reference 7, which compared the double fin-tube and central fin-tube configurations without taking into account the effects of header heat rejection and weight as well as pressure drops in the radiator tubes, showed a similar percentage increase in Q_{rej}/W by reducing δ_s/δ_a. This data, which was for a 1-megawatt, 1700° R, beryllium radiator, indicated a 6-percent weight advantage for the double fin tube at a $\delta_s/\delta_a = 0.5$ and a 28 percent advantage at $\delta_s/\delta_a = 0$ over the central fin-tube configuration.

The conductance parameter obtained at maximum heat rejection per unit weight is plotted as a function of inside tube diameter for a $\delta_s/\delta_a = 0.5$ for both geometries in figure 12. Results obtained for δ_s/δ_a other than 0.5 showed very little variation in the optimum value of N_c. Both the 500-

kilowatt and 1-megawatt examples are shown with the double fin-tube results yielding the higher value of N_c for a specific choice of inside tube diameter. It is also noted that the values of N_c obtained for the 500-kilowatt columbium radiator are somewhat larger than those obtained for the 1-megawatt beryllium radiator. Reference 7 indicated the double fin-tube configuration reached maximum Q_{rej}/W at much larger values of N_c than those obtained in this report.

Radiator Geometry

Planform area. - The planform area of the double fin-tube geometry is shown plotted in figure 13 for the two power levels chosen for this investigation. This figure illustrates the calculated variations of planform area with L/R_o ratio, conductance parameter N_c, and tube side-wall thickness to armor thickness ratio δ_s/δ_a for the two power cycles for peak Q_{rej}/W conditions. The two inside tube diameters used for the results shown in figure 13 correspond to near minimum weight conditions. Reducing the tube side-wall thickness ratio for peak L/R_o ratios results in only a small variation in planform area for a constant value of N_c but results in a sizable decrease in L/R_o. However, it should be kept in mind that the actual fin length l is not decreasing that rapidly since the fin length is being increased by the amount $\delta_a - \delta_s$ as δ_s/δ_a approaches zero. The decrease in L/R_o (which is a measure of the tube center-to-center distance) as δ_s/δ_a decreases causes a reduction in tube block effectiveness (due to reduced Q_b) and an increase in fin effectiveness (fig. 6) that result in only a small variation in total fin-tube effectiveness for a specific choice of N_c. This accounts for the negligible variation of planform area with varying δ_s/δ_a. Similar results are obtained for the other inside tube diameters investigated.

Comparison of the planform area results of the double fin-tube geometry with those of the central fin-tube geometry indicates good agreement as shown by figure 14. The planform area obtained for the central fin tube is less than that of the double fin tube for internal tube diameters greater than 1/2 inch for the 500-kilowatt columbium radiator. At the 3/8-inch diameter, which corresponds to near minimum weight, the two fin-tube geometries agreed to within 4 percent. For the 1-megawatt beryllium system, the double fin tube has the larger planform area at tube diameters greater than 5/8 inch. At near optimum weight corresponding to a 5/8-inch diameter, the central fin-tube geometry offers only a small savings in planform area. The planform area obtained for the double fin-tube geometry in reference 7 for the 1-megawatt radiator is much greater than that obtained from the comparison calculations of this report. This is brought about because the conductance parameter at maximum Q_{rej}/W for the case of reference 7 was larger than the values obtained in this report. Figure 13 verifies that increasing conductance parameter N_c results in increased planform area.

Fin thickness. - The effect of reducing the tube side-wall ratio δ_s/δ_a on fin thickness is shown for the two examples in figure 15 for peak Q_{rej}/W conditions at near optimum inside tube diameter. In both cases, reducing

δ_s/δ_a results in a sizable decrease in fin thickness at constant N_c. Accompanying this decrease in fin thickness is a reduction in L/R_o and thus tube spacing. The magnitude of the fin thickness obtained for the two sample cases at optimum values of N_c (fin thickness t is greater than 0.020 in. for the columbium radiator and greater than 0.035 in. for the beryllium radiator) resulted in values of fin thickness that are reasonable and should satisfy structural and fabricational requirements.

The comparison of the fin thickness obtained for the double fin-tube configuration indicates an increasing total fin thickness with increasing values of tube side wall to armor ratio δ_s/δ_a throughout the range of D_i investigated for both power levels (fig. 16). Curves are given for fin thickness at maximum Q_{rej}/W for both geometries and both system power levels with central and double fin-tube $\delta_s/\delta_a = 0.5$ cases agreeing closely for the 1 megawatt radiator.

Panel aspect ratio. - Radiator panel aspect ratio, which is defined as the ratio of panel width $\overline{W}$ to the tube length Z for the four panel radiator of figure 1, is shown plotted in figure 17 for the two double fin-tube example cases. The aspect ratio of a panel is seen to decrease as the tube block side-wall ratio δ_s/δ_a decreases at a constant N_c. The decrease in aspect ratio with reduced δ_s/δ_a is primarily a result of the reduced L/R_o since reductions in δ_s/δ_a had little effect on planform area as shown by figure 13. These results can be indicated by inspection of equation (48), which describes planform area and length, and equation (23), which describes the total panel width $\overline{W}$. The reduction in aspect ratio at constant planform area is explained by the calculations which showed that as δ_s/δ_a gets smaller the number of tubes and the tube length increase as the L/R_o ratio decreases. This was accompanied by a large reduction in the working fluid inlet tube velocity.

The panel aspect ratio showed practically no difference between the central fin-tube and double fin-tube configurations as indicated in figures 18(a) and (b) for the 500-kilowatt and 1-megawatt systems, respectively.

Number of tubes. - The number of radiator tubes required was found to increase substantially as the tube block side-wall ratio decreased. The 500-kilowatt columbium radiator with a tube inside diameter of 3/8 inch had 298, 337, and 430 tubes for δ_s/δ_a ratios of 1.0, 0.5, and 0, respectively, at maximum heat rejection per unit weight. The 1-megawatt beryllium radiator using a tube inside diameter of 5/8 inch had 223, 250, and 302 tubes for δ_s/δ_a ratios of 1.0, 0.5, and 0, respectively, at maximum Q_{rej}/W.

For simplicity and reliability of fabrication it is desirable to reduce the number of tubes. A sizable reduction in the number of tubes without much reduction in Q_{rej}/W can be had by just increasing the size of the tube inside diameter. For the 500-kilowatt columbium radiator with tube block side-wall ratio set at 0.5, a 3/8-inch inside tube diameter required 337 tubes whereas a 1/2-inch inside diameter results in 206 tubes. This reduction in the number of tubes results in only a 2-percent decrease in Q_{rej}/W. The 1-megawatt beryl-

lium radiator with δ_s/δ_a set at 0.5 required 250 tubes for a 5/8-inch inside tube diameter whereas a 3/4-inch inside diameter required just 182 tubes. This reduction resulted in only a 3-percent decrease in Q_{rej}/W. Similar reductions in the number of tubes can be obtained at values of δ_s/δ_a equal to 0 and 1.0 with small reductions in Q_{rej}/W.

Comparison of the number of tubes for the central and double fin-tube radiators at maximum Q_{rej}/W for the 500-kilowatt case indicated the central fin-tube geometry required 308 tubes compared to 298 tubes for the double fin-tube $\delta_s/\delta_a = 1.0$ radiator at an inside tube diameter of 3/8 inch. This trend also held for the 1-megawatt case for which the central fin-tube required 226 tubes compared to 223 for the double fin-tube $\delta_s/\delta_a = 1.0$ radiator.

Interpolation of results. - If the values of the ratio of δ_s/δ_a other than the three values chosen for this investigation (0, 0.5, and 1) are designated by forthcoming meteoroid bumper results, additional points may be obtained from curves faired through the calculated points to obtain intermediate values of panel aspect ratio $\overline{W}/Z$, fin thickness t, radiator planform area A_p, and radiator heat rejection per unit weight Q_{rej}/W.

SUMMARY OF RESULTS

An analysis of the double fin-tube configuration with variable tube block side-wall thickness and a comparison with a comparable central fin-tube radiator for the sample cases of a 1-megawatt beryllium radiator and a 500-kilowatt columbium radiator for a 500-day mission time and probability of no puncture P(0) of 0.995 showed that

1. A substantial increase in radiator heat rejection per unit weight is possible for the double fin-tube geometry if the tube block side-wall thickness can be reduced to less than 75 percent of that required for normal armor thickness.

2. The double fin-tube configuration with ratio of tube block side-wall thickness to normal armor thickness of 0.5 offers an 11 and 8 percent weight savings over the central fin-tube geometry for the 500-kilowatt and 1-megawatt cases, respectively. This corresponds to 15.0 pounds per kilowatt for the 500-kilowatt case and 4.68 pounds per kilowatt for the 1-megawatt case considered herein compared to 16.7 and 4.83 pounds per kilowatt for the central fin-tube 500-kilowatt and 1-megawatt cases, respectively.

3. The percent weight savings is increased to 39 and 32 percent for the 500-kilowatt and 1-megawatt cases, respectively, if the ratio of tube block side-wall thickness to normal armor thickness is set at 0. In this case, the corresponding radiator specific weights would be 10.2 and 3.50 pounds per kilowatt for the double fin-tube geometry and 16.7 and 4.83 pounds per kilowatt for the central fin-tube geometry.

4. The double fin-tube configuration reached maximum heat rejection per

unit weight for the 1-megawatt system at a conductance parameter of 0.75 whereas maximum heat rejection per unit weight for the central fin-tube geometry occurred at 0.63. These values for the 500-kilowatt case were 0.63 and 0.75, respectively, for the double and central fin-tube. However, the conductance parameter associated with maximum heat rejected per unit weight decreases with decreasing inside tube diameter for both the double and central fin-tube radiators.

5. The double fin-tube radiator reaches maximum heat rejected per unit weight for a tube inside diameter in the range from 3/8 to 1/2 inch for the 500-kilowatt case, and from 1/2 to 5/8 inch for the 1-megawatt case.

6. The physical dimensions of the double fin-tube radiator (planform area, panel aspect ratio, number of tubes, inside tube diameter, and fin thickness) can be varied over a fairly wide range without seriously decreasing the radiator heat rejection per unit weight.

7. The fin thickness obtained for maximum heat rejection per unit weight for the double fin-tube geometry is of reasonable fabricational and structural magnitude (greater than 0.02 in. for the 500 kw columbium radiator and greater than 0.035 in. for the 1 Mw beryllium radiator).

8. The values of planform area and panel aspect ratio obtained for the double and central fin-tube geometries were in close agreement regardless of the choice of tube block side-wall ratio near the minimum weight condition. Comparison of the total fin thickness for the two geometries agreed well at a tube block side-wall thickness ratio of 0.5, but showed considerable variations at side-wall ratios of 1.0, and 0.

9. Reduction of the tube block side-wall thickness ratio substantially increases the number of radiator tubes at maximum heat rejection per unit weight. However, the number of tubes can be reduced to the values corresponding to the central fin-tube geometry by increasing the value of D_i above that for maximum heat rejection per unit weight. The weight penalty involved is only several percent.

Lewis Research Center
National Aeronautics and Space Administration
Cleveland, Ohio, August 12, 1964

REFERENCES

1. Krebs, R. P., Winch, D. M., and Lieblein, S.: Analysis of a Megawatt Level Direct Condenser-Radiator. Prog. in Astronautics and Aeronautics. Vol. 11 - Power Systems for Space Flight, Academic Press, Inc., 1963, pp. 475-504.

2. Ross, Daniel P., Ray, Edward, and Haller, Henry C.: Heat Rejection from Space Vehicles. Preprint 60-39, Am. Astronautical Soc., 1960.

3. Walker, C. L., Smith, C. R., and Gritton, D. G.: Weight Optimization of Heat Rejection Systems for Space Application. Proc. of Heat Transfer and Fluid Mech. Inst., 1960, pp. 244-259.

4. Haller, Henry C., Wesling, Gordon C., and Lieblein, Seymour: Heat-Rejection and Weight Characteristics of Fin-Tube Space Radiators with Tapered Fins. NASA TN D-2168, 1964.

5. Hefner, R. J.: Design Procedure for a Minimum Weight Space Radiator. ORNL 60-8-21, Oak Ridge Nat. Lab., Aug. 1960.

6. Krebs, R. P., Haller, H. C., and Auer, B. M.: Analysis and Design Procedures for a Flat, Direct-Condensing, Central Finned-Tube Radiator. NASA TN D-2474, 1964.

7. Haller, H. C.: Comparison of Heat Rejection and Weight Characteristics of Several Radiator Fin-Tube Configurations. NASA TN D-2385, 1964.

8. McMillan, A. R.: An Investigation of the Penetration of Hyper-Velocity Projectiles into Composite Laminates. Proc. Sixth Symposium on Hypervelocity Impact, Vol. 3, Aug. 1963, pp. 309-356.

9. Loeffler, I. J., Lieblein, Seymour, and Clough, Nestor: Meteoroid Protection for Space Radiators. Prog. in Astronautics and Aeronautics. Vol. 11 - Power Systems for Space Flight, Academic Press, Inc., 1963, pp. 551-579.

10. Lieblein, S., Clough, N., and McMillan, A. R.: Hypervelocity Impact Damage Characteristics in Armored Space Radiator Tubes. NASA TN D-2472, 1964.

11. Sparrow, E. M., and Minkowycz, W. J.: Heat-Transfer Characteristics of Several Finned-Tube Radiators. NASA TN D-1435, 1962.

12. Jakob, Max: Heat Transfer. Vol. 2. John Wiley & Sons, Inc., 1957.

13. Sparrow, E. M., and Eckert, E. R. G.: Radiant Interaction Between Fin and Base Surfaces. Jour. Heat Transfer (Trans. ASME), ser. C, vol. 84, no. 1, Feb. 1962, pp. 12-18.

14. Lockhart, R. W., and Martinelli, R. C.: Proposed Correlation of Data for Isothermal Two Phase, Two-Component Flow in Pipes. Chem. Eng. Prog., vol. 45, no. 1, Jan. 1949, pp. 39-45; discussion, pp. 45-48.

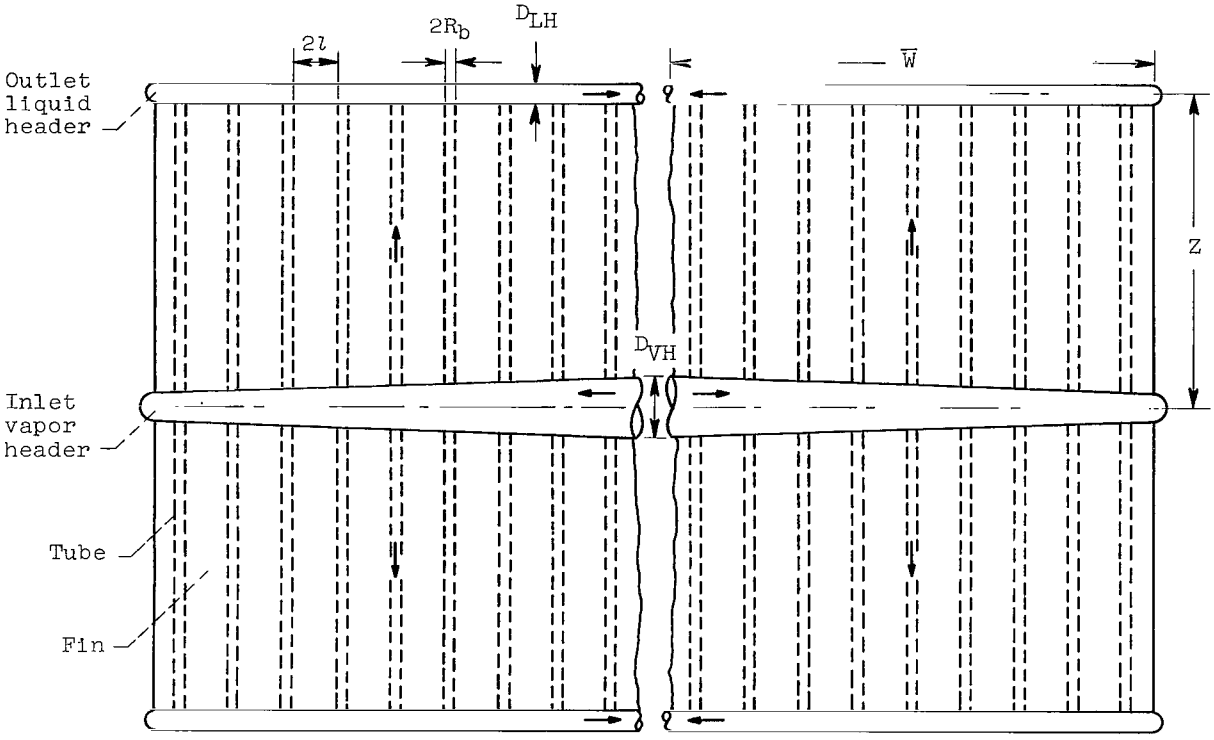

Figure 1. - Schematic of four-panel radiator configuration.

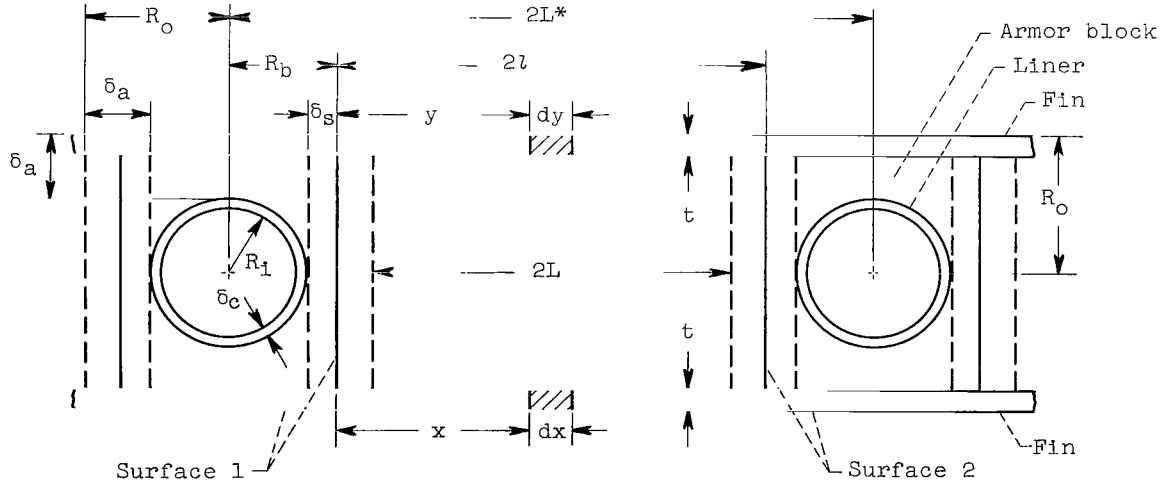

Figure 2. - Double fin-tube geometry with variable side-wall thickness.

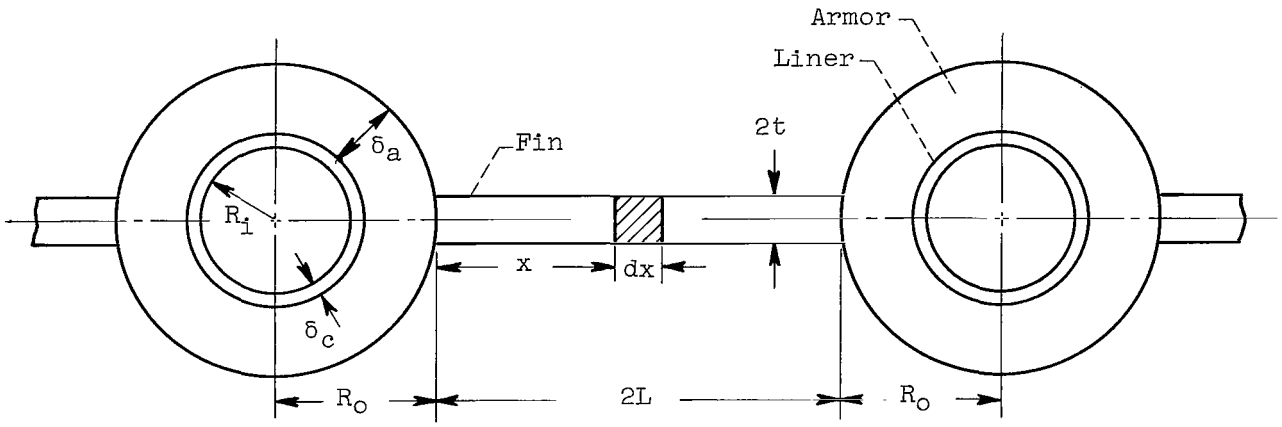

Figure 3. - Central fin-tube geometry.

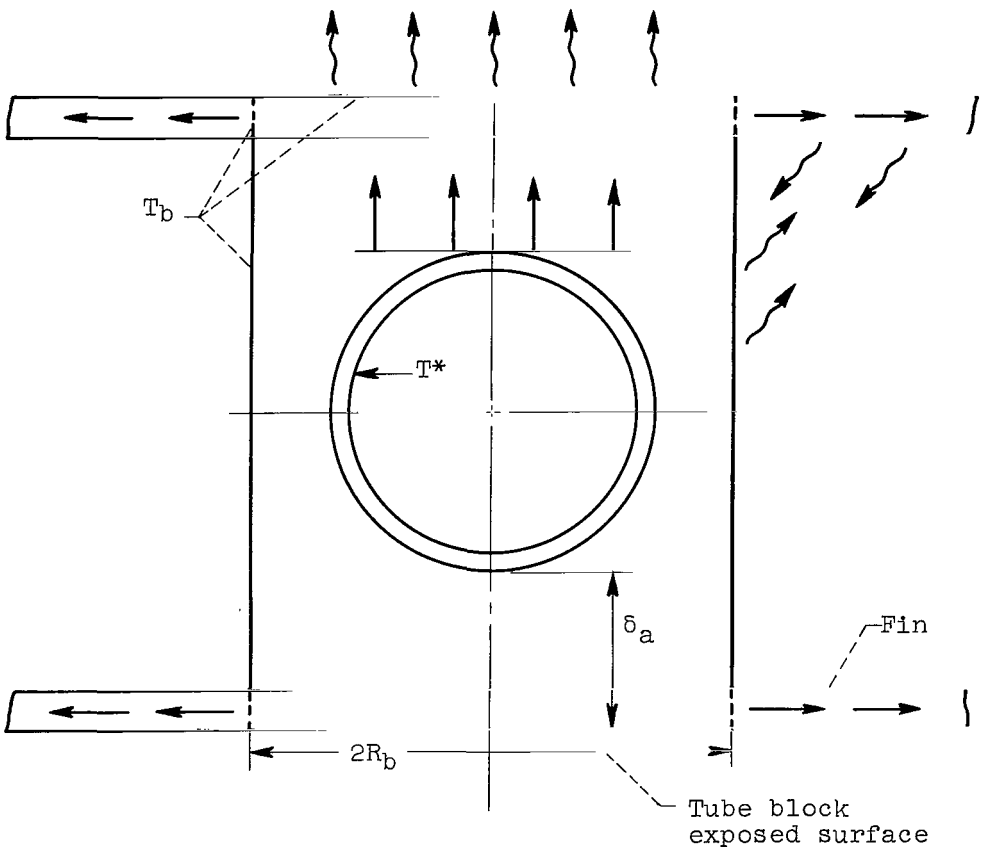

Figure 4. - Assumed radiator heat-transfer paths.

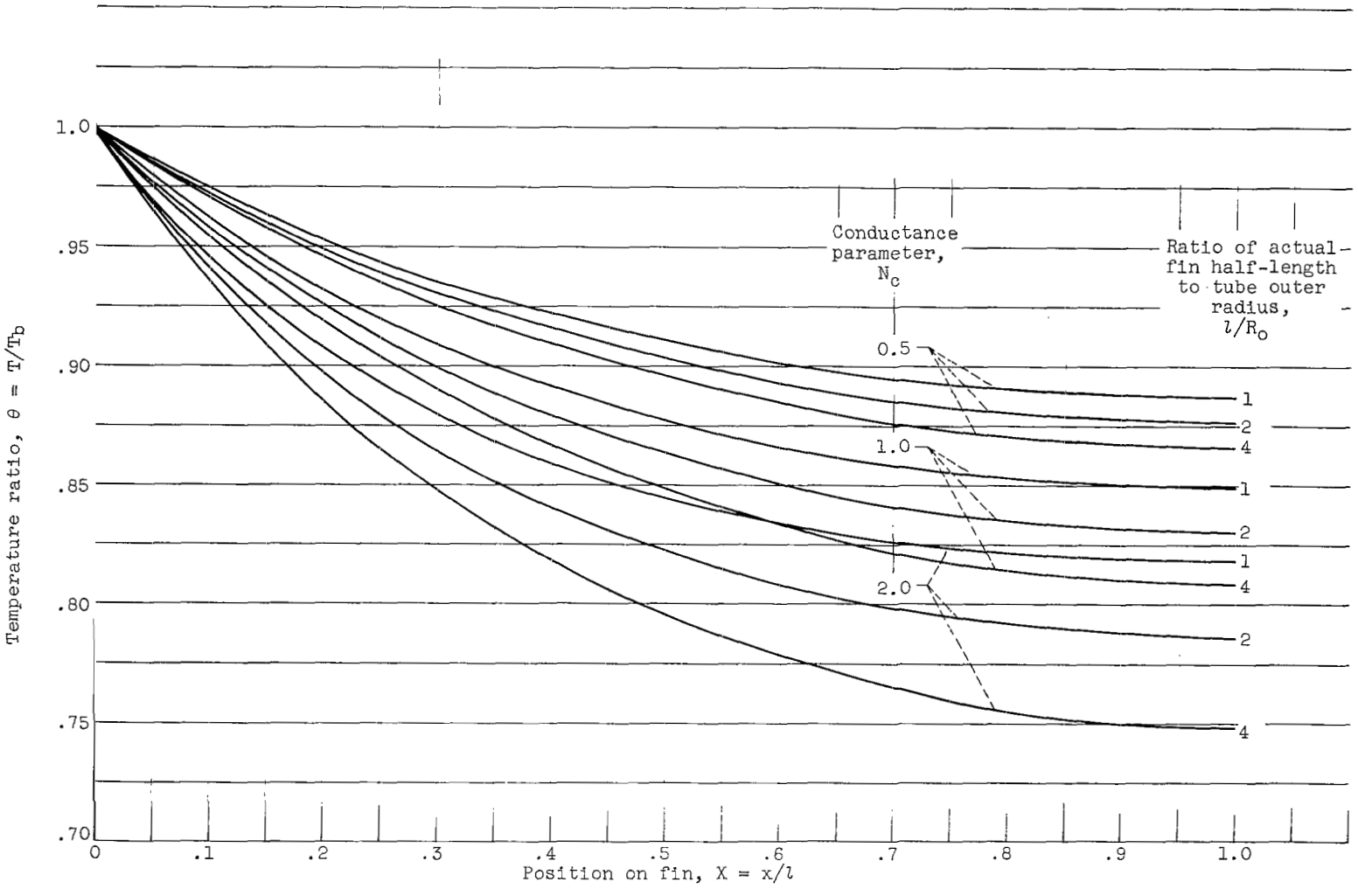

Figure 5. - Fin temperature profile; closed sandwich fin tube.

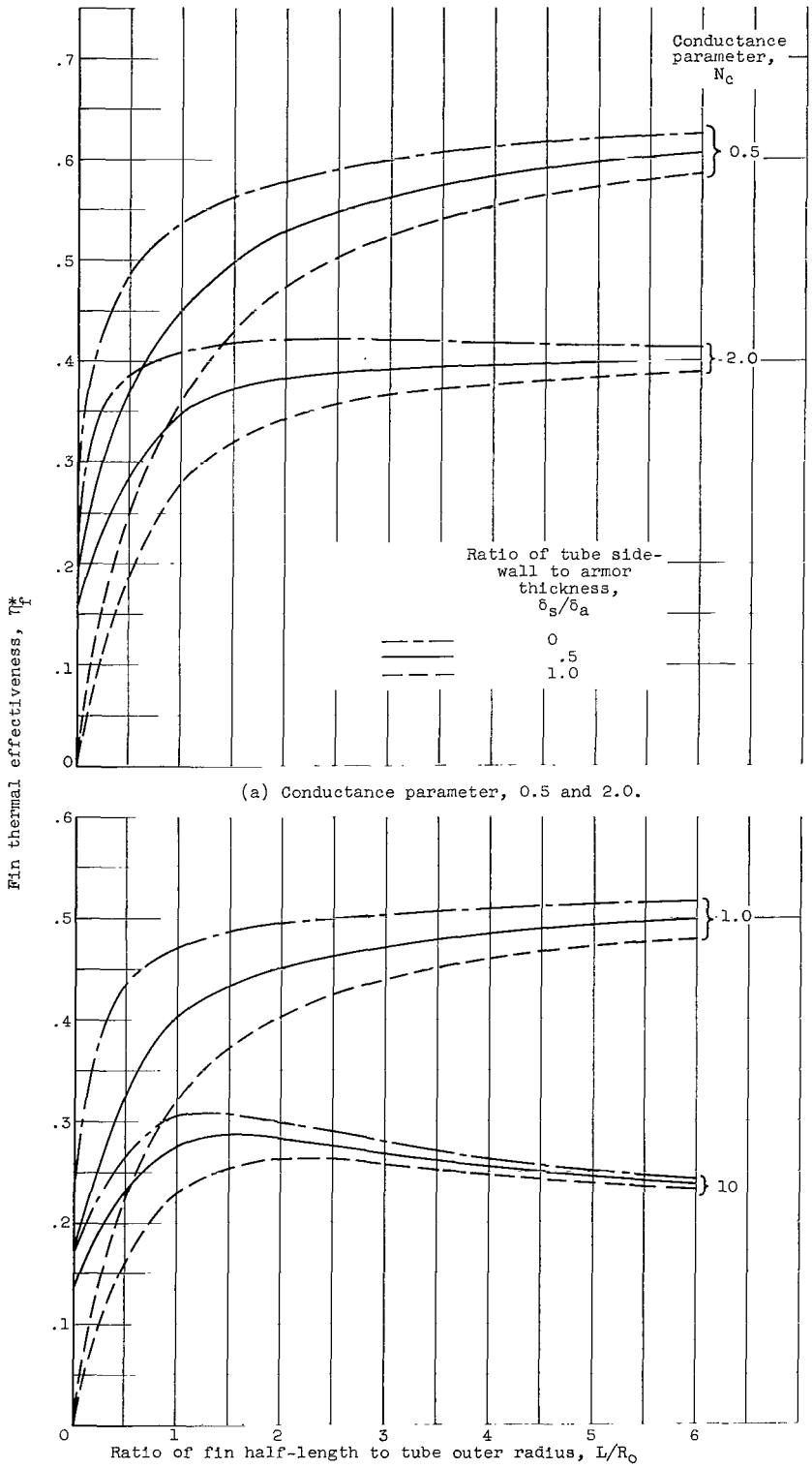

(a) Conductance parameter, 0.5 and 2.0.

(b) Conductance parameter, 1.0 and 10.

Figure 6. - Fin effectiveness; double fin-tube geometry. Powerplant output, 500 kilowatts; temperature at radiator inlet, 1700° R; inside tube diameter, 3/4 inch; columbium radiator.

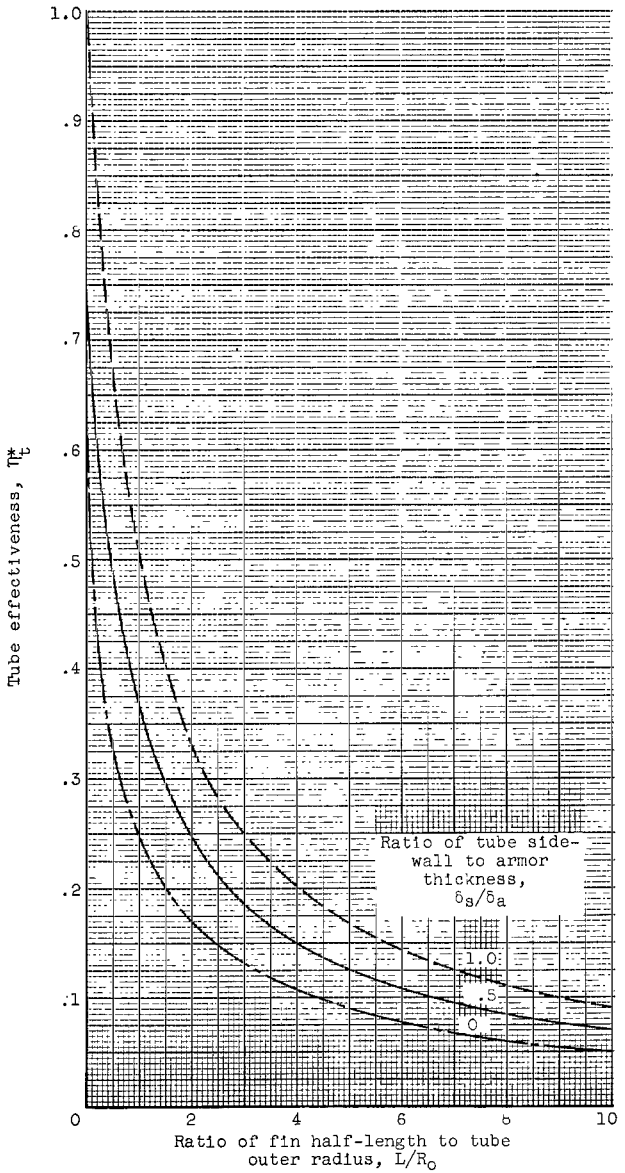

Figure 7. - Tube effectiveness; double fin-tube geometry. Powerplant output, 500 kilowatts; temperature at radiator inlet, 1700° R; inside diameter, 3/4 inch; columbium radiator.

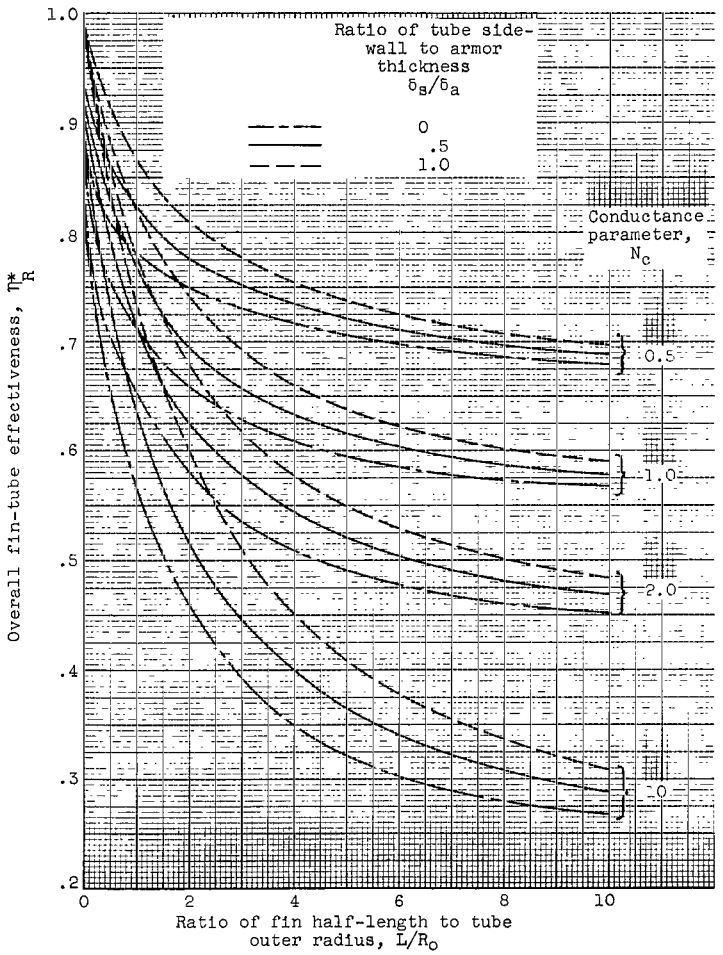

Figure 8. - Overall fin-tube effectiveness; double fin-tube geometry. Powerplant output, 500 kilowatts; temperature at radiator inlet, 1700° R; inside tube diameter, 3/4 inch; columbium radiator.

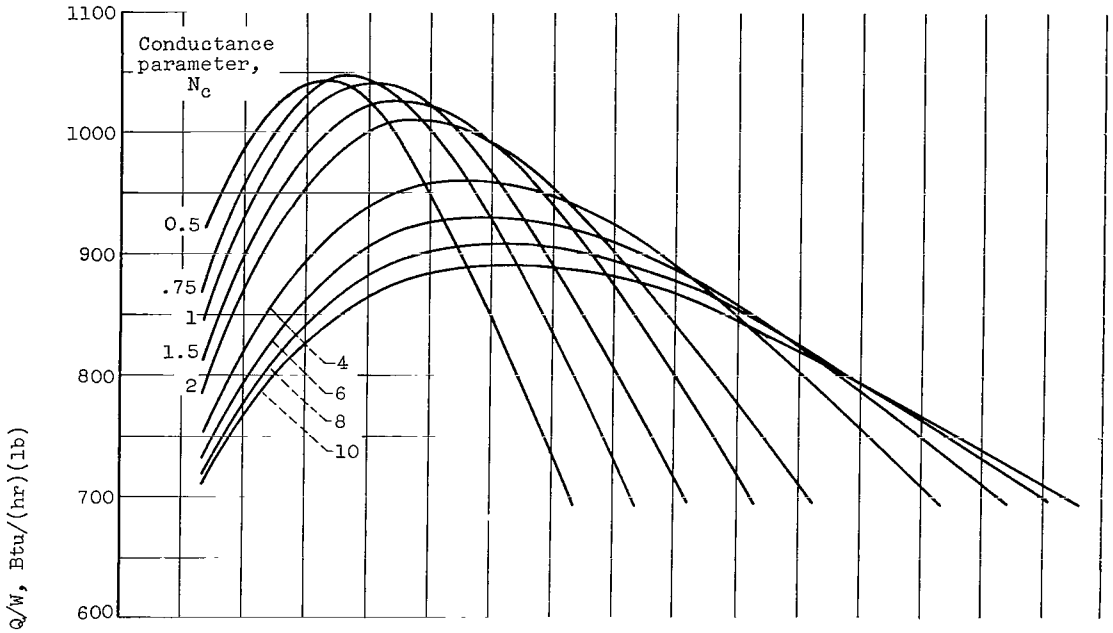

(a) Powerplant output, 500 kilowatts; inside tube diameter, 3/8 inch; columbium radiator.

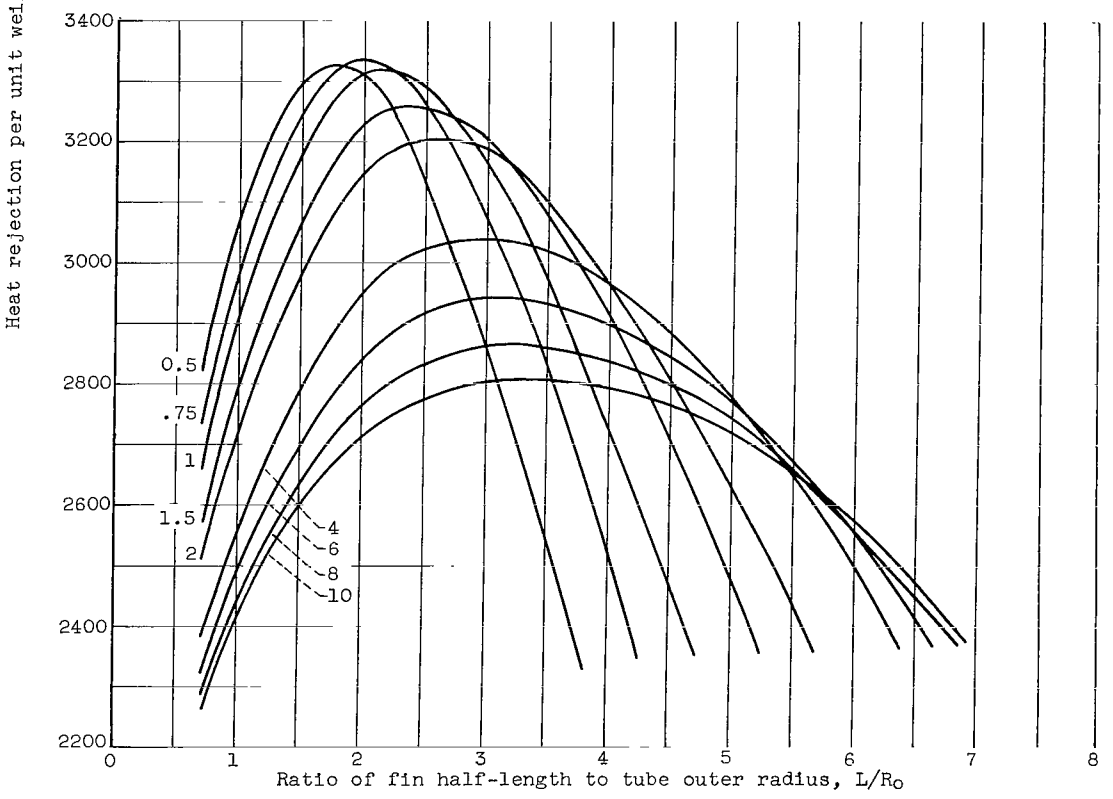

(b) Powerplant output, 1 megawatt; inside tube diameter, 5/8 inch; beryllium radiator.

Figure 9. - Heat rejection per unit weight characteristics; double fin-tube geometry. Temperature at radiator inlet, 1700° R; ratio of tube side-wall to armor thickness, 0.5.

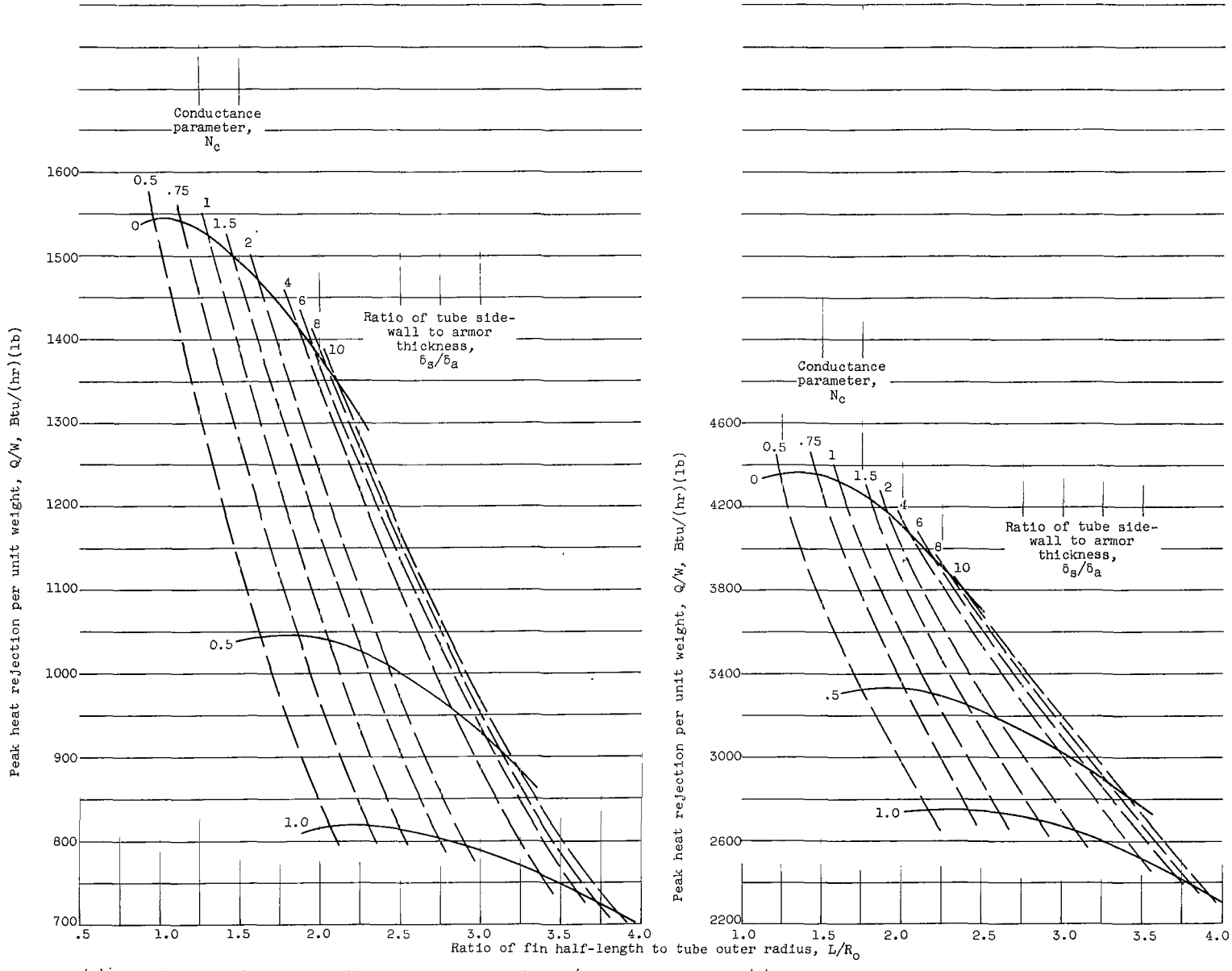

(a) Powerplant output, 500 kilowatts; inside tube diameter, 3/8 inch; columbium radiator.

(b) Powerplant output, 1 megawatt; inside tube diameter, 5/8 inch; beryllium radiator.

Figure 10. - Comparison of peak heat rejection characteristics of double fin-tube geometry with variable tube block side wall. Temperature at radiator inlet, 1700° R.

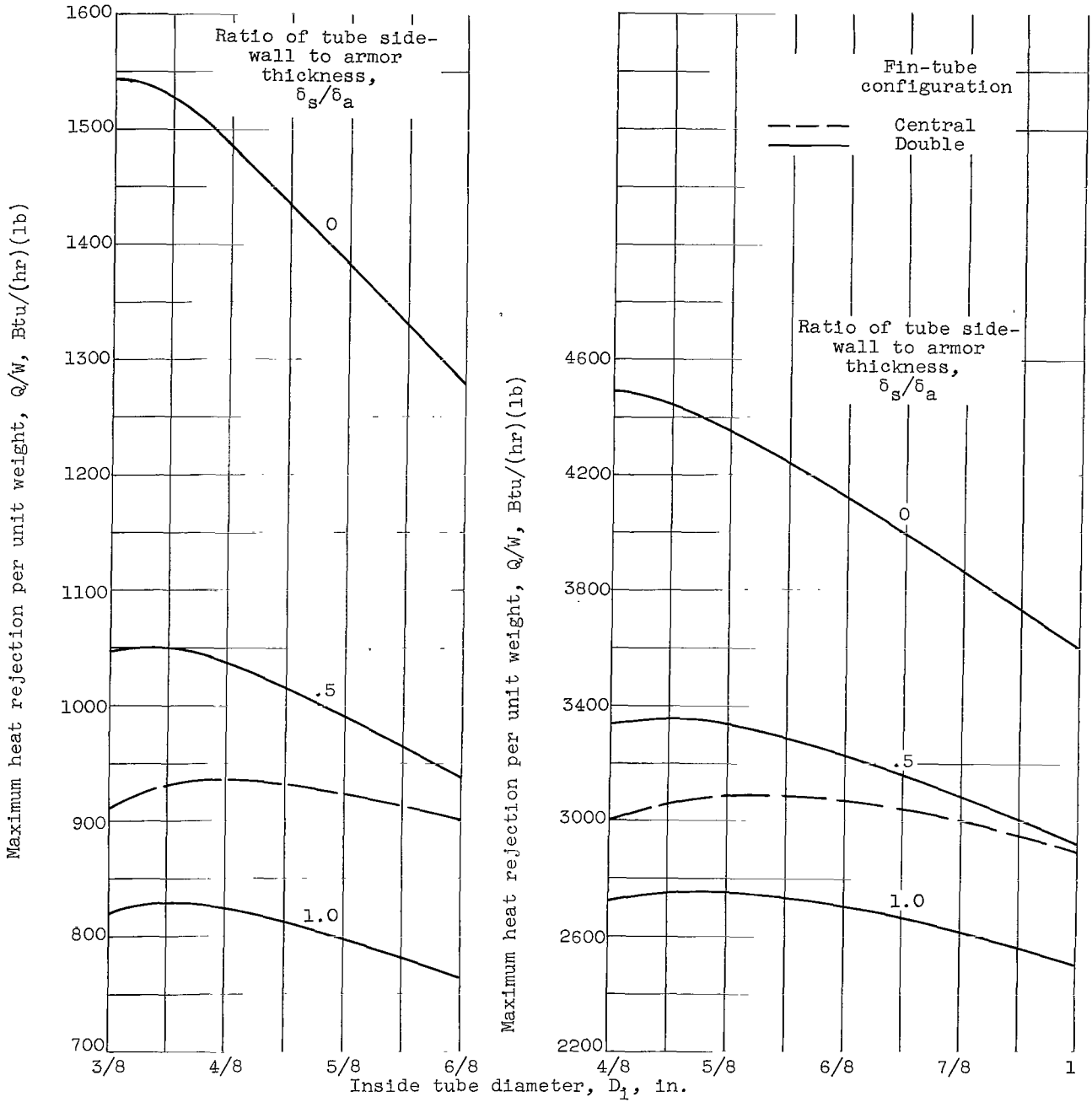

(a) Powerplant output, 500 kilowatts; columbium radiator.

(b) Powerplant output, 1 megawatt; beryllium radiator.

Figure 11. - Maximum heat rejection per unit weight. Temperature at radiator inlet, 1700° R.

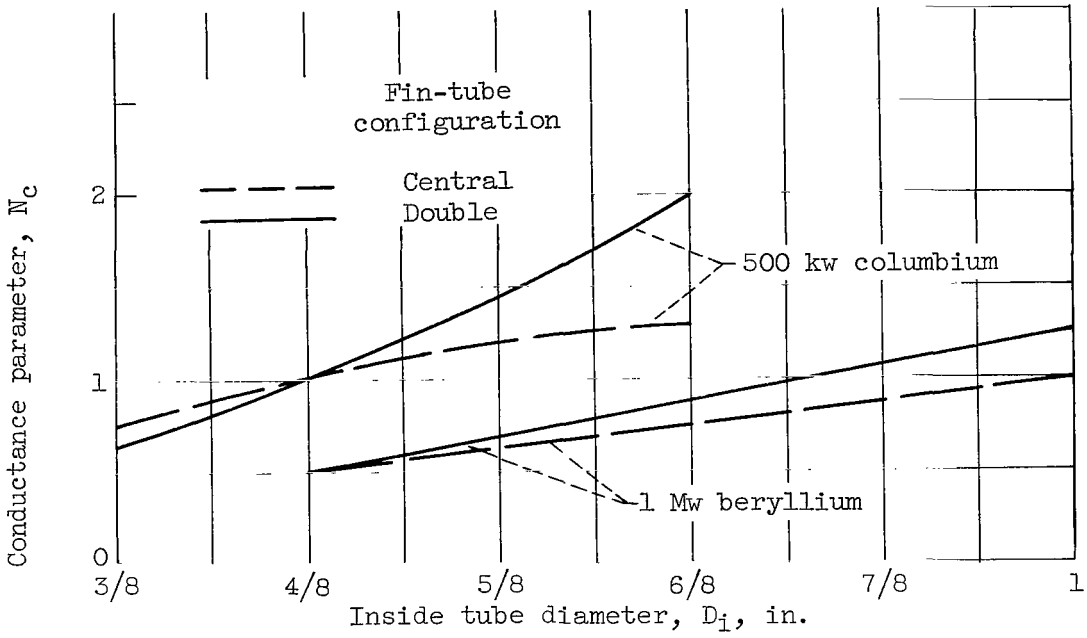

Figure 12. - Conductance parameter at maximum heat rejection per unit weight.

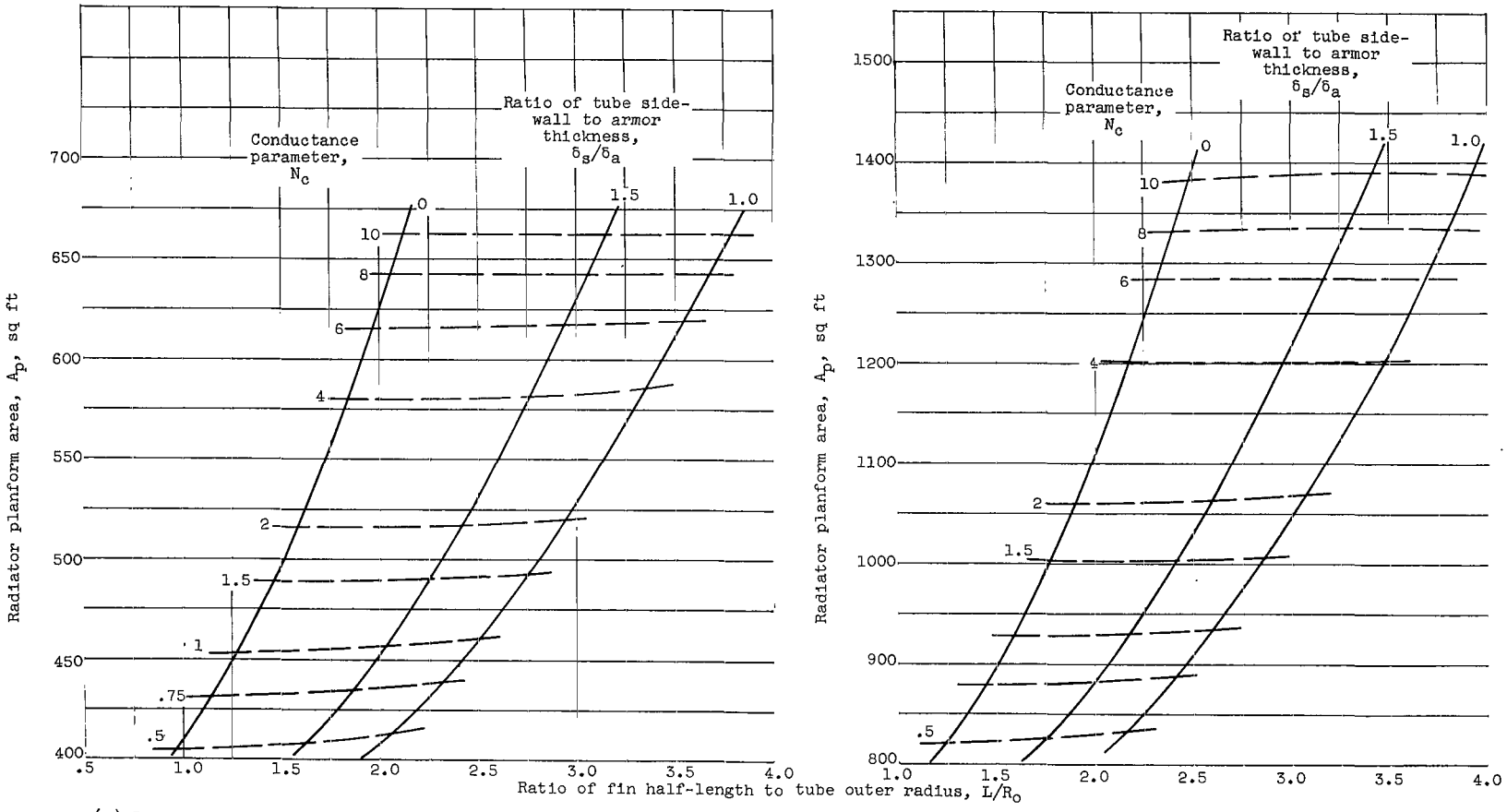

(a) Powerplant output, 500 kilowatts; inside tube diameter, 3/8 inch; columbium radiator.

(b) Powerplant output, 1 megawatt; inside tube diameter, 5/8 inch; beryllium radiator.

Figure 13. - Comparison of radiator planform area at peak heat rejection per unit weight; double fin-tube geometry. Temperature at radiator inlet, 1700° R.

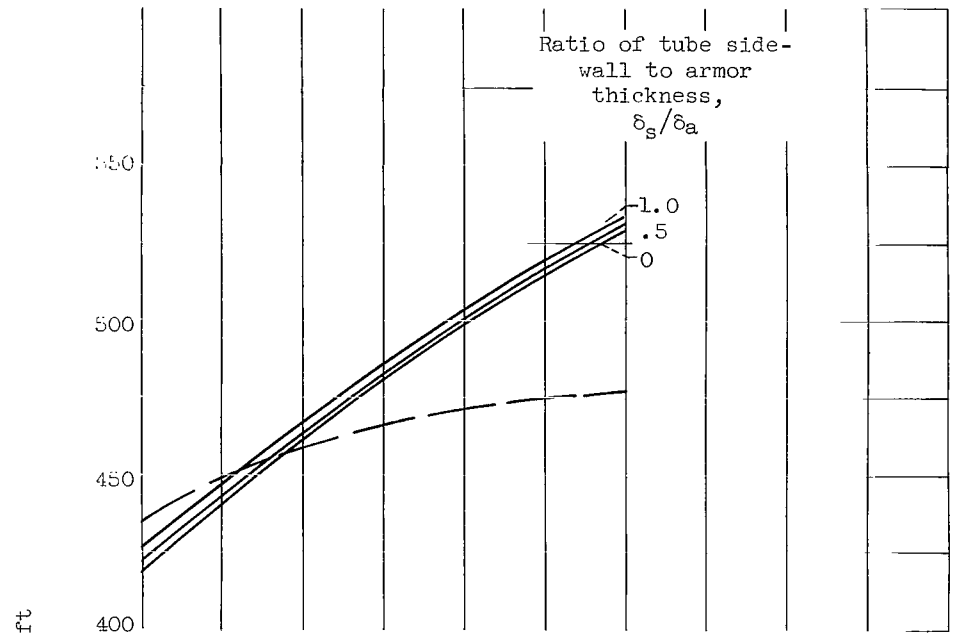

(a) Powerplant output, 500 kilowatts; columbium radiator.

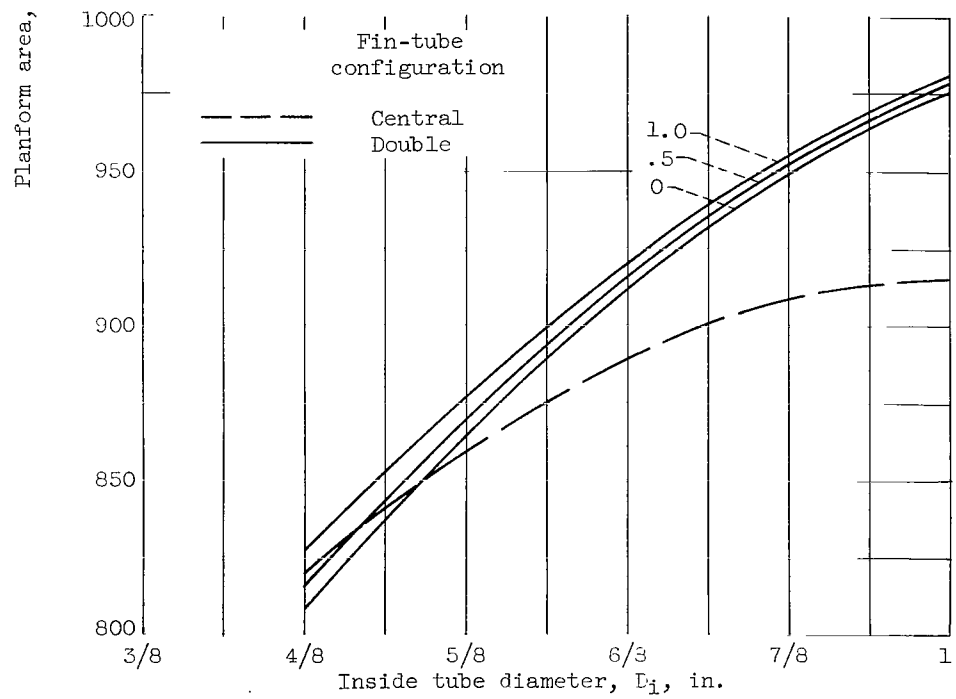

(b) Powerplant output, 1 megawatt; beryllium radiator.

Figure 14. - Planform area comparison at maximum heat rejection per unit weight for double and central fin-tube radiators. Temperature at radiator inlet, 1700° R.

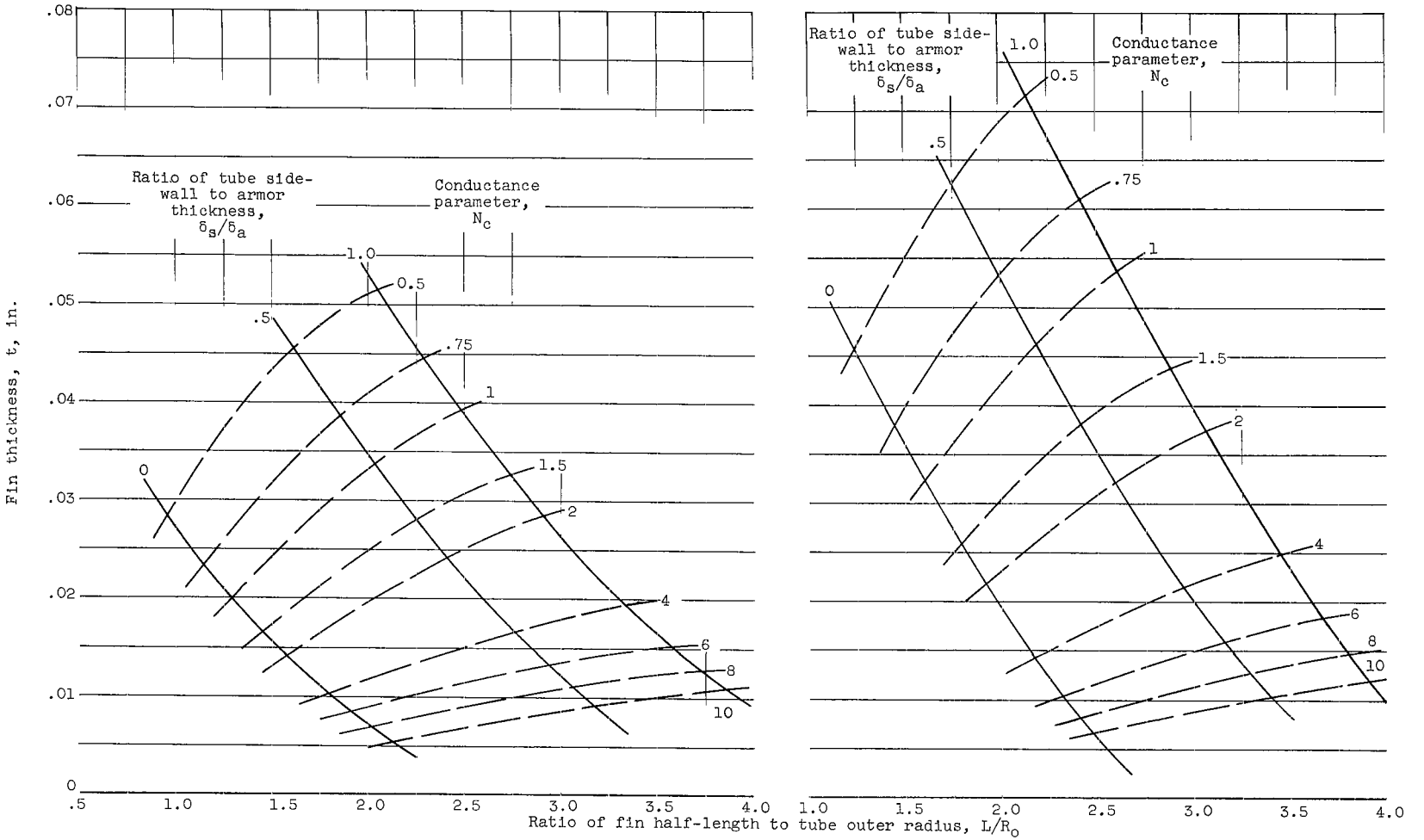

(a) Powerplant output, 500 kilowatts; inside tube diameter, 3/8 inch; columbium radiator.

(b) Powerplant output, 1 megawatt; inside tube diameter, 5/8 inch; beryllium radiator.

Figure 15. - Radiator fin thickness at peak heat rejection per unit weight; double fin-tube geometry. Temperature at radiator inlet, 1700° R.

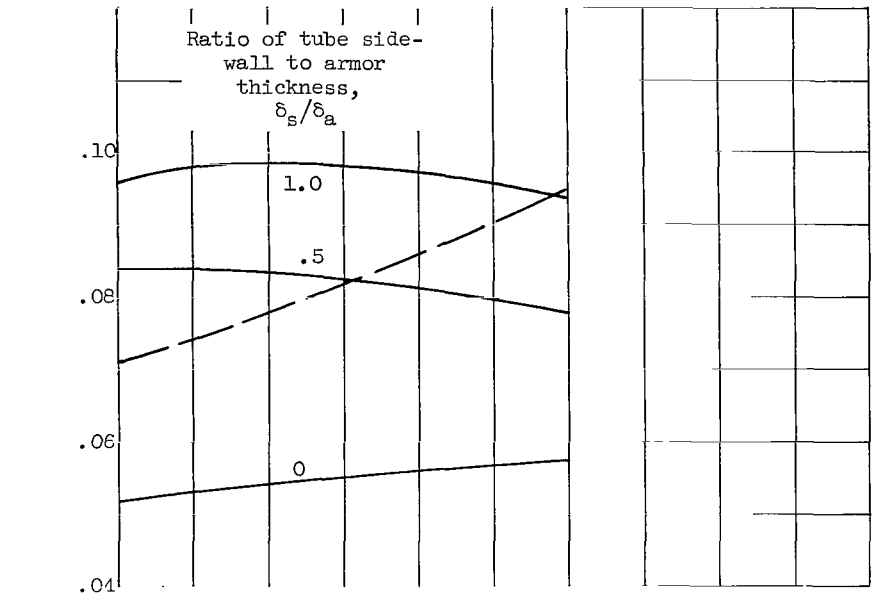

(a) Powerplant output, 500 kilowatts.

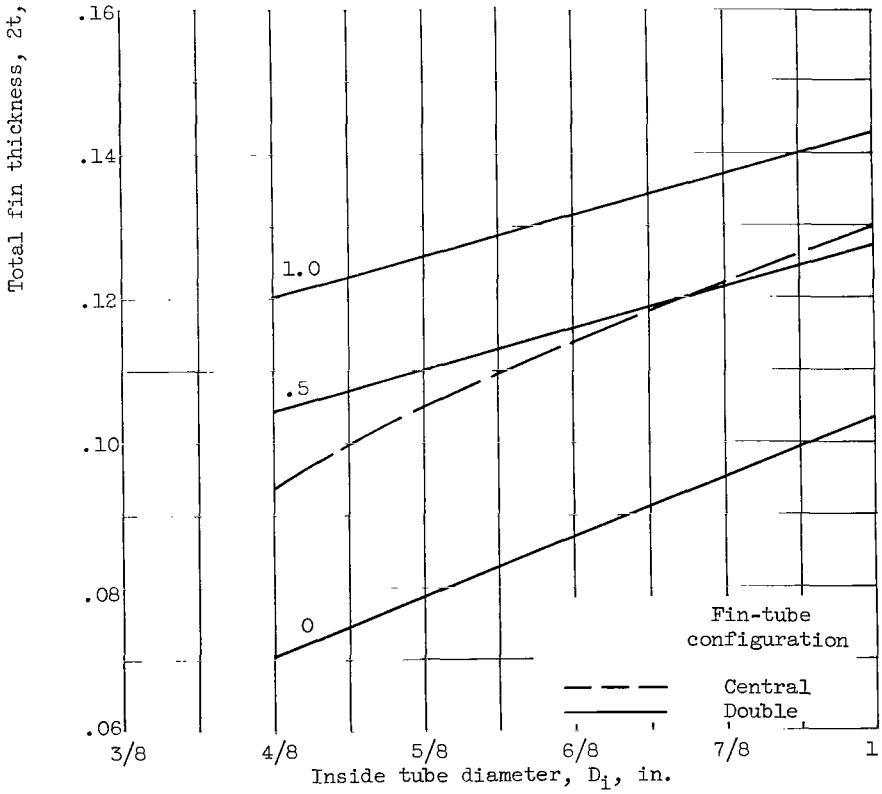

(b) Powerplant output, 1 megawatt.

Figure 16. - Total fin thickness at maximum heat reduction per unit weight for double and central fin-tube radiators. Temperature at radiator inlet, 1700° R.

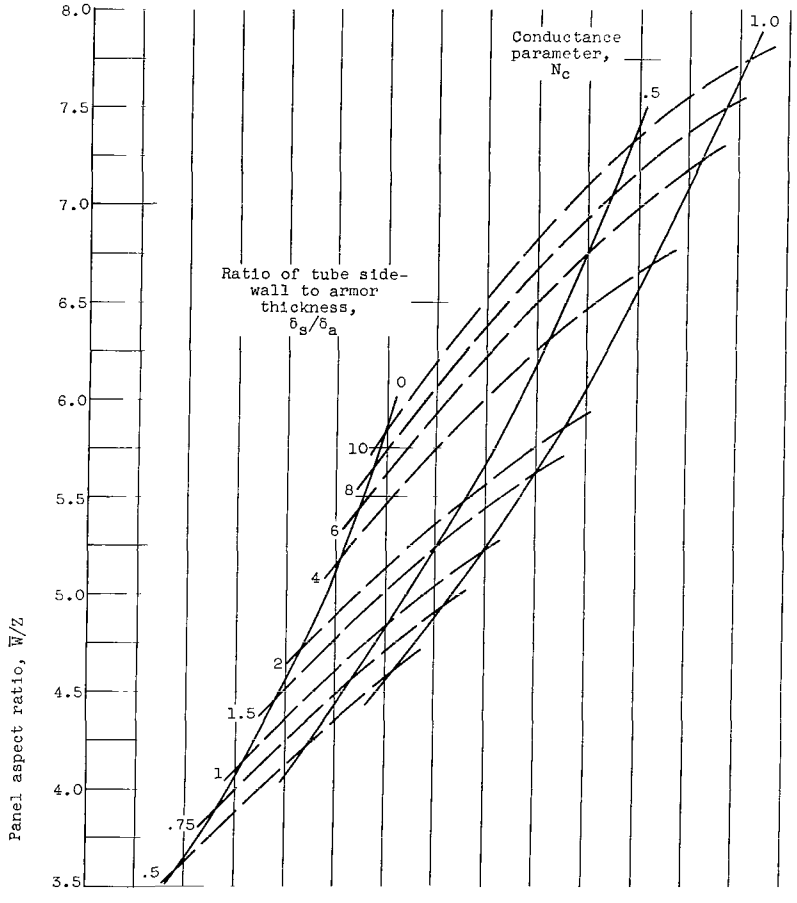

(a) Powerplant output, 500 kilowatts; inside tube diameter, 3/8 inch; columbium radiator.

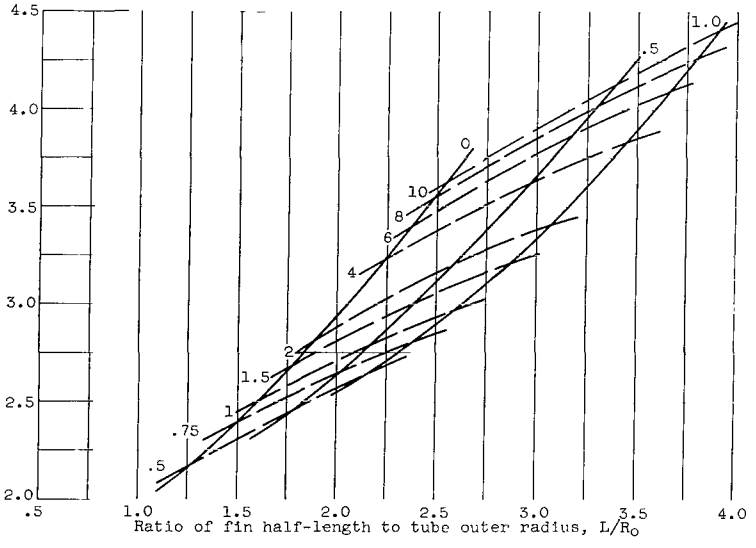

(b) Powerplant output, 1 megawatt; inside tube diameter, 5/8 inch; beryllium radiator.

Figure 17. - Radiator panel aspect ratio at peak heat rejection per unit weight; double fin-tube geometry; four panels. Temperature at radiator inlet, 1700° R.

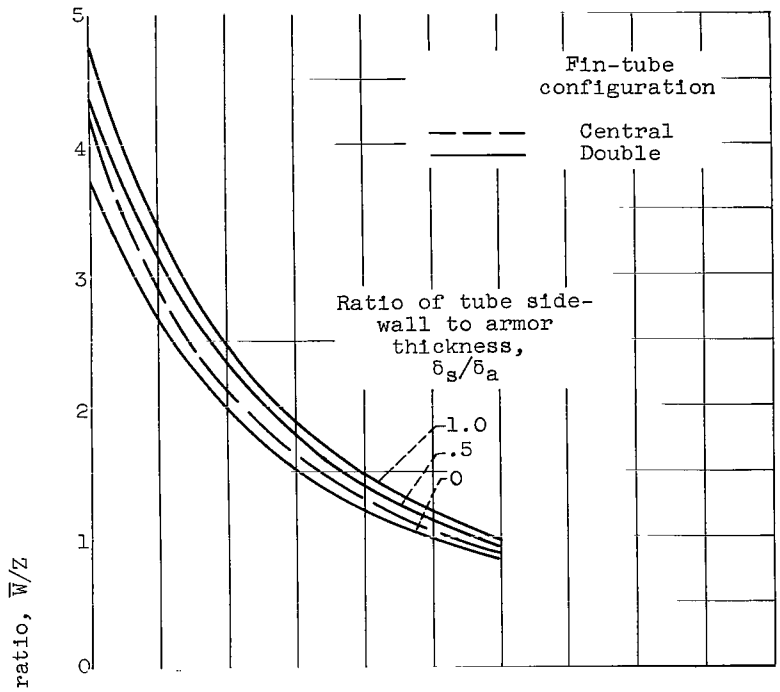

(a) Powerplant output, 500 kilowatts.

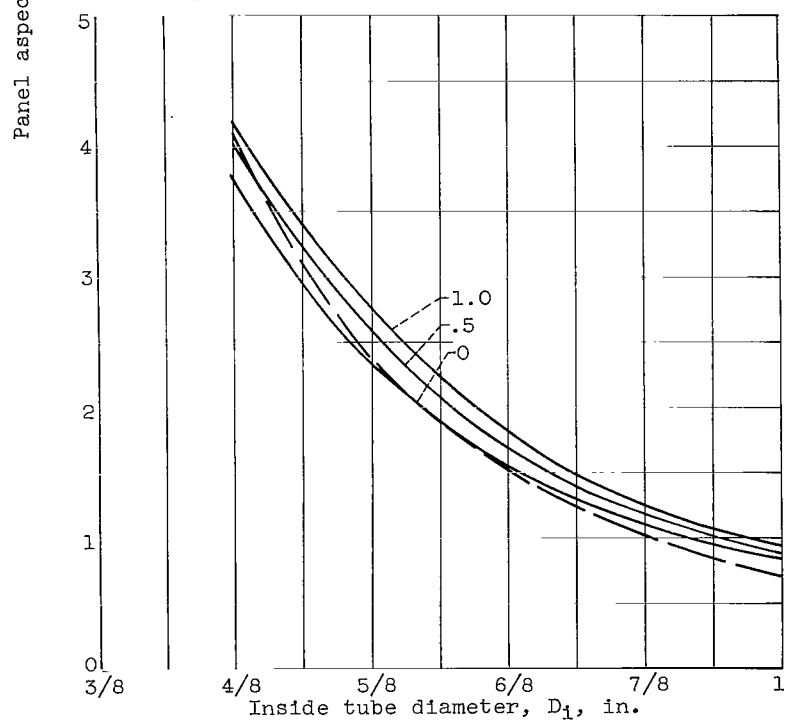

(b) Powerplant output, 1 megawatt.

Figure 18. - Panel aspect ratio comparison at maximum heat rejection per unit weight for double and central fin-tube radiators. Temperature at radiator inlet, 1700° R.

"The aeronautical and space activities of the United States shall be conducted so as to contribute . . . to the expansion of human knowledge of phenomena in the atmosphere and space. The Administration shall provide for the widest practicable and appropriate dissemination of information concerning its activities and the results thereof."

—NATIONAL AERONAUTICS AND SPACE ACT OF 1958

NASA SCIENTIFIC AND TECHNICAL PUBLICATIONS

TECHNICAL REPORTS: Scientific and technical information considered important, complete, and a lasting contribution to existing knowledge.

TECHNICAL NOTES: Information less broad in scope but nevertheless of importance as a contribution to existing knowledge.

TECHNICAL MEMORANDUMS: Information receiving limited distribution because of preliminary data, security classification, or other reasons.

CONTRACTOR REPORTS: Technical information generated in connection with a NASA contract or grant and released under NASA auspices.

TECHNICAL TRANSLATIONS: Information published in a foreign language considered to merit NASA distribution in English.

TECHNICAL REPRINTS: Information derived from NASA activities and initially published in the form of journal articles.

SPECIAL PUBLICATIONS: Information derived from or of value to NASA activities but not necessarily reporting the results of individual NASA-programmed scientific efforts. Publications include conference proceedings, monographs, data compilations, handbooks, sourcebooks, and special bibliographies.

Details on the availability of these publications may be obtained from:

SCIENTIFIC AND TECHNICAL INFORMATION DIVISION

NATIONAL AERONAUTICS AND SPACE ADMINISTRATION

Washington, D.C. 20546